Dynamics of in vivo ASC speck formation

Paola Kuri,[1] Nicole L. Schieber,[2] Thomas Thumberger,[4] Joachim Wittbrodt,[4] Yannick Schwab,[2,3] and Maria Leptin[1,5,6]

[1]Directors' Research Unit, [2]Cell Biology and Biophysics Unit, and [3]Electron Microscopy Core Facility, European Molecular Biology Laboratory, Heidelberg, Germany
[4]Centre for Organismal Studies, Heidelberg University, Heidelberg, Germany
[5]Institute of Genetics, University of Cologne, Cologne, Germany
[6]European Molecular Biology Organization, Heidelberg, Germany

Activated danger or pathogen sensors trigger assembly of the inflammasome adaptor ASC into specks, large signaling platforms considered hallmarks of inflammasome activation. Because a lack of in vivo tools has prevented the study of endogenous ASC dynamics, we generated a live ASC reporter through CRISPR/Cas9 tagging of the endogenous gene in zebrafish. We see strong ASC expression in the skin and other epithelia that act as barriers to insult. A toxic stimulus triggered speck formation and rapid pyroptosis in keratinocytes in vivo. Macrophages engulfed and digested that speck-containing, pyroptotic debris. A three-dimensional, ultrastructural reconstruction, based on correlative light and electron microscopy of the in vivo assembled specks revealed a compact network of highly intercrossed filaments, whereas pyrin domain (PYD) or caspase activation and recruitment domain alone formed filamentous aggregates. The effector caspase is recruited through PYD, whose overexpression induced pyroptosis but only after substantial delay. Therefore, formation of a single, compact speck and rapid cell-death induction in vivo requires a full-length ASC.

Introduction

Inflammasomes are large, supramolecular structures that signal the detection of danger or pathogenic stimuli by specific pattern-recognition receptors, including some NOD-like receptor (NLR) family members (Broz and Dixit, 2016; Sharma and Kanneganti, 2016). Inflammasome signaling ultimately leads to the activation of the effector caspase-1 through proximity-induced, auto-proteolytic cleavage (Hauenstein et al., 2015). Activated caspase-1 can proteolytically process cytokines as well as trigger pyroptosis, a proinflammatory form of regulated cell death, through cleavage of Gasdermin D (Man and Kanneganti, 2016). During pyroptosis, cells swell after the N-terminal domain of Gasdermin D assembles into pores in the plasma membrane, leading to its rupture and the release of intracellular contents and membrane vesicles (Vande Walle and Lamkanfi, 2016; Vince and Silke, 2016). The adaptor molecule apoptosis-associated speck-like protein containing a CARD (ASC) is central to the inflammasome assembly process (Hoss et al., 2017). ASC is composed of two protein–protein interaction domains of the death-domain superfamily, a pyrin domain (PYD_A) and a caspase activation and recruitment domain ($CARD_A$) joined by a flexible linker (de Alba, 2009). This enables ASC to interact with both PYD-containing receptors and the CARD-containing procaspase-1, thus bridging sensor and effector molecules (Broz and Dixit, 2016).

Upon activation, inflammasome-forming receptors oligomerize and nucleate the prion-like aggregation of ASC, enabling the subsequent clustering of caspase-1 (Cai et al., 2014; Lu et al., 2014). During this process, ASC is rapidly depleted from its steady-state, homogeneous cellular distribution and self-associates to form a single punctum inside the cell of ∼1 µm in diameter, called a speck (Masumoto et al., 1999; Fernandes-Alnemri et al., 2007). The fast and irreversible assembly of ASC into specks maximizes the amount of activated caspase-1, ensuring high signal amplification (Kagan et al., 2014; Broz and Dixit, 2016).

Structural methods used to analyze specks in vitro showed that ASC assembles into filaments in which PYD_A forms a rigid, cylindrical core, whereas $CARD_A$ is directed outward through a flexible attachment (Lu et al., 2014; Sborgi et al., 2015). The external orientation of $CARD_A$, in addition to enabling the recruitment of downstream signaling elements, allows intra- and interfilament cross-linking through $CARD_A$–$CARD_A$ interactions. Indeed, recent cell culture studies showed that preventing $CARD_A$ interactions by single-point mutagenesis (Dick et al., 2016) or use of an intracellular alpaca antibody fused to a fluorescent protein (Schmidt et al., 2016) abolishes speck formation, but not a PYD_A filament assembly. However, whether in vivo, assembled specks also share this cross-linked filament arrangement has not been analyzed with structural methods.

Specks can be visualized using light microscopy by expressing ASC fused to a fluorescent protein from a transgene

Correspondence to Maria Leptin: mleptin@uni-koeln.de

Abbreviations used: CARD, caspase activation and recruitment domain; CDS, coding DNA sequence; CLEM, correlative light and electron microscopy; dpf, days postfertilization; EV, entry vector; EVL, enveloping layer; gDNA, genomic DNA; hphs, hours post–heat shock; HSE, heat-shock element; NLR, NOD-like receptors; PIT, pore-induced intracellular trap; PYD, pyrin domain; sgRNA, single-guide RNA; TEM, transmission electron microscopy; tGFP, turbo-GFP.

The Rockefeller University Press
J. Cell Biol. Vol. 216 No. 9 2891–2909
https://doi.org/10.1083/jcb.201703103

(Fernandes-Alnemri et al., 2007; Cheng et al., 2010). The switch from a diffuse signal throughout the cell to one single bright point is considered a readout and a proxy for inflammasome activation (Stutz et al., 2013; Sester et al., 2015; Beilharz et al., 2016; Tzeng et al., 2016). However, experimentally expressed constructs increase the cellular concentration of ASC and, given the protein's high tendency to aggregate if overexpressed (Hoss et al., 2017), the risk that speck formation occurs without an inflammatory stimulus also increases. The aforementioned study by Schmidt et al. (2016) represented the first time that endogenous ASC was visible using live cell imaging, rather than immunofluorescence. However, because speck formation is abolished by the use of the alpaca antibody, this tool cannot be used to assess speck formation in vivo.

Inflammasome function has mainly been studied in cells of the innate immune system, such as macrophages. However, many pathogens and toxic agents first enter the body through epithelia that form the interface between body and environment, which evidently requires innate immune-surveillance mechanisms (Yazdi et al., 2010). In spite of that, little is known about the role of the inflammasome and ASC in these or other tissues, such as endothelium or connective tissue, which are also composed of cells that contribute to a global inflammatory response (Yazdi et al., 2010; Peeters et al., 2015; Santana et al., 2016). For example, although ASC is present in mammalian epidermis (Feldmeyer et al., 2010) and acts as a tumor suppressor in keratinocytes (Drexler et al., 2012), whether speck formation leads to pyroptosis in those cells is unknown. Studying the responses of native tissues in vivo using murine models, however, is challenging because of limited imaging accessibility.

The zebrafish (*Danio rerio*) is a genetically and optically accessible model organism for studying diseases and for drug screening (Renshaw and Trede, 2012; van der Vaart et al., 2012; Torraca et al., 2014; Lin et al., 2016), in which in vivo innate immune responses can be studied in the context of a whole organism (Renshaw and Trede, 2012; Angosto and Mulero, 2014; Kuri et al., 2016). The zebrafish genome contains more than 10 times as many NLR genes as the mouse or human genomes (Stein et al., 2007; Hansen et al., 2011; Howe et al., 2016). However, it has only one gene encoding ASC (named *pycard*, here referred to as *asc*) with a PYD–CARD domain structure; a zebrafish homologue of *caspase-1* (named *caspa*) has also been identified. Although *caspa* has an N-terminal PYD domain, instead of a CARD domain, when cotransfected with zebrafish ASC in mammalian cells, the two proteins colocalize in a single speck (Masumoto et al., 2003).

We use zebrafish to study ASC function in tissues, such as skin, in which inflammasome signaling has not been addressed in vivo. The transparency of the zebrafish makes this model especially well-suited to study ASC-mediated inflammasome formation using speck formation as the readout. For this purpose, we generated a line in which the endogenous *asc* was tagged with GFP using CRISPR/Cas9 technology, allowing body-wide, in vivo analysis of speck formation.

This tool, together with an *asc*-inducible expression system with which we visualize the ultrastructure of specks formed in vivo, revealed that speck formation in keratinocytes can occur within the nucleus and that macrophages engulf pyroptotic cellular debris. Furthermore, the expression of the separate ASC domains shows both PYD_A and $CARD_A$ cluster in filamentous aggregates. PYD_A aggregates are sufficient to elicit cell death at a reduced rate, showing $CARD_A$ is required both for maximal speck clustering and cell death efficiency. Finally, by generating a Caspase-1 orthologue knockout, we conclude that speck formation unleashes Caspase-dependent pyroptosis in keratinocytes in vivo.

Results

Tissue-specific expression of ASC

ASC has been shown to be expressed in the skin, digestive tract, bone marrow, and peripheral blood leukocytes, among other tissues in humans (Masumoto et al., 2001), and most myeloid lineage cell lines also express *asc* constitutively (Hoss et al., 2017). However, no encompassing analysis addressing the spatial distribution of its expression sites within an organism has been made. To investigate the role of ASC in vivo, we first characterized gene and protein expression in zebrafish by RT-PCR in situ hybridization and immunofluorescence with a newly generated antibody against zebrafish ASC. The expression of *asc* is detectable from the morula stage onward, and adult hematopoietic tissues also express *asc* (Fig. S1 A). In 3-d-post-fertilization (dpf) larvae, *asc* RNA is present throughout the epidermis and in the area around the gills (Fig. 1 A and Fig. S1 B), where it has previously been reported to have a role in pharyngeal arch development (Masumoto et al., 2003). Sections showed expression in internal tissues, such as the intestinal epithelium and individual *asc*-expressing cells in the brain (Fig. 1, B and C; and Fig. S1, C–G″). The lateral line system and some internal tissues, such as the notochord and muscle, lacked ASC. Immunostainings showed ASC presence in the epidermis from 1 to at least 5 dpf (Fig. S1, I–O). Transgenic tissue-specific markers identified the ASC-expressing cells in the skin as both enveloping layer (EVL) and basal keratinocytes (Fig. 1, D and D′). In these cells, the protein is seen both in the cytoplasm and the nucleus (Fig. 1 E). All macrophages express ASC, as do most neutrophils (Fig. 1, F and G), but not all cells labeled by the myeloid lineage reporter *spi1b* express ASC (Fig. 1 H).

Endogenous ASC and specks visualized in vivo in a knock-in transgenic line

To be able to study ASC in vivo, we generated a transgenic CRISPR knock-in line through homology-dependent repair in which the endogenous protein is fused with GFP, called *Tg(asc:asc-EGFP)* (Fig. S1, P–R). In agreement with the aforementioned results, transgenic embryos have ASC–GFP throughout the entire epidermis, in nuclear and cytoplasmic compartments as well as in the intestinal epithelium (Fig. 2, A–C″). ASC–GFP is also expressed in myeloid cells (Fig. 2 D). Microglia, the tissue-resident macrophages of the brain (Peri and Nüsslein-Volhard, 2008) were ASC^+, as were cells in the caudal hematopoietic tissue; many (but not all) of which were labeled by the *spi1b* reporter transgene. At all stages examined, muscle cells and other internal tissues were devoid of GFP.

We observed the sporadic appearance of GFP specks in the epidermis of *Tg(asc:asc-EGFP)* larvae (Video 1). Without exception, specks were contained in dead or dying cells, as shown in brightfield images in which these cells were rounded and dislodged from the rest of the epithelium (Fig. 3, A–C). The reason for spontaneous speck formation in these examples is unclear. To determine whether inflammatory stimuli could trigger speck formation in epidermal cells, we exposed *Tg(asc:asc-EGFP)* embryos to high concentrations of copper sulfate

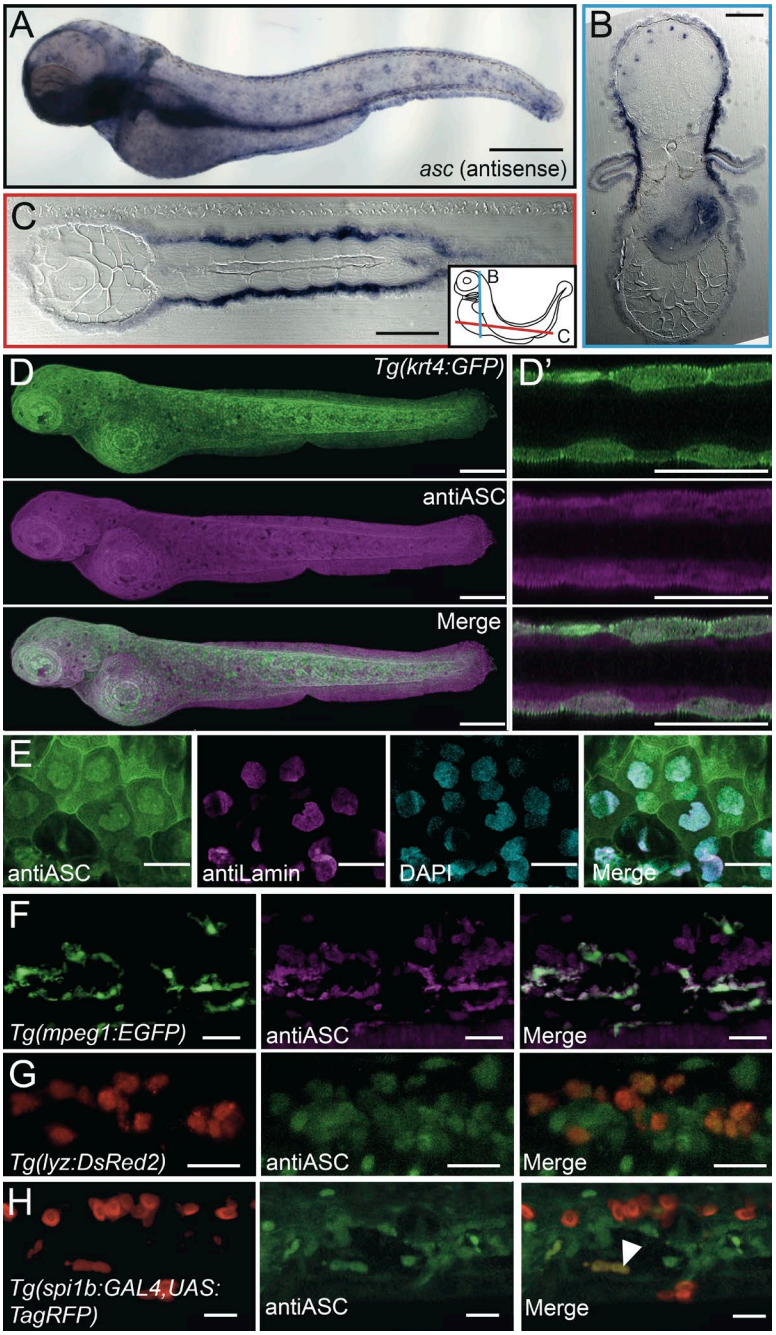

Figure 1. ***asc* is expressed during zebrafish early development.** *asc* whole-mount, in situ hybridization (*wish*) of 3-dpf zebrafish larvae (A) with cross (B) and longitudinal (C) sectioning of plastic embedded *wish* sample showing expression in epidermis, intestinal epithelium, and cells located in the brain. Bars: (full larvae) 300 µm; (sections) 100 µm. Immunostaining of ASC in 3-dpf *Tg(krt4:GFP)* larva (D). Optical cross section of lateral fin showing GFP expression in the EVL and ASC expression on both epidermal layers (D′). WT 3-dpf larva immunostained for ASC, together with nuclear envelope marker lamin and DAPI shows its nuclear and cytoplasmic localization (E). Immunostaining of 3-dpf *Tg(mpeg1:EGFP)* (F), *Tg(lyz:DsRed2)* (G), and *Tg(spi1b :GAL4,UAS:TagRFP)* (H) larvae showing expression of ASC in macrophages, neutrophils, and a single myeloid cell in the caudal hematopoietic tissue (H, white arrowhead). Bars: (full larvae) 300 µm; (all others) 30 µm.

($CuSO_4$), a compound toxic to zebrafish larvae (Olivari et al., 2008; d'Alençon et al., 2010; Hernandez et al., 2011). The epidermis of these larvae showed signs of stress, with many deformed cells forming a rugged, instead of a smooth, epithelium and had significantly increased numbers of specks (Fig. 2 D). Cells containing a speck were rounded and dislodged from the rest of the epithelium, which is indicative of cell death. However, not all abnormal epidermal cells had specks (Fig. 2, E and E′), suggesting $CuSO_4$ exposure triggers a range of stress symptoms, and speck formation may occur as an indirect consequence of $CuSO_4$-induced toxicity to the skin. Because toxicity-induced speck formation in the skin resulted in undesired side effects, making this an inadequate system with which to address the dynamics and consequences of speck formation in vivo, we tested other, more-direct means of triggering speck formation.

Speck formation in vivo is induced by NLR or ASC overexpression

When ASC is present at endogenous concentrations, activated members of the NLR protein family, among other receptors, can trigger speck formation. Under overexpression conditions, however, the propensity of ASC to spontaneously aggregate in cultured cells is well documented (Masumoto et al., 1999; Stutz et al., 2013; Sester et al., 2015). We, therefore, tested whether these stimuli resulted in speck formation in live fish. Overexpressing a PYD-containing zebrafish NLR (ENSDARP00000137642.1) lacking the leucine-rich repeat domain led to ASC–GFP speck formation in epidermal cells of the *Tg(asc:asc-EGFP)* line, showing that the GFP-tagged, endogenous ASC responds appropriately to its direct stimulus (Fig. 4 A and Video 2). We also used an overexpression system, based on the construct

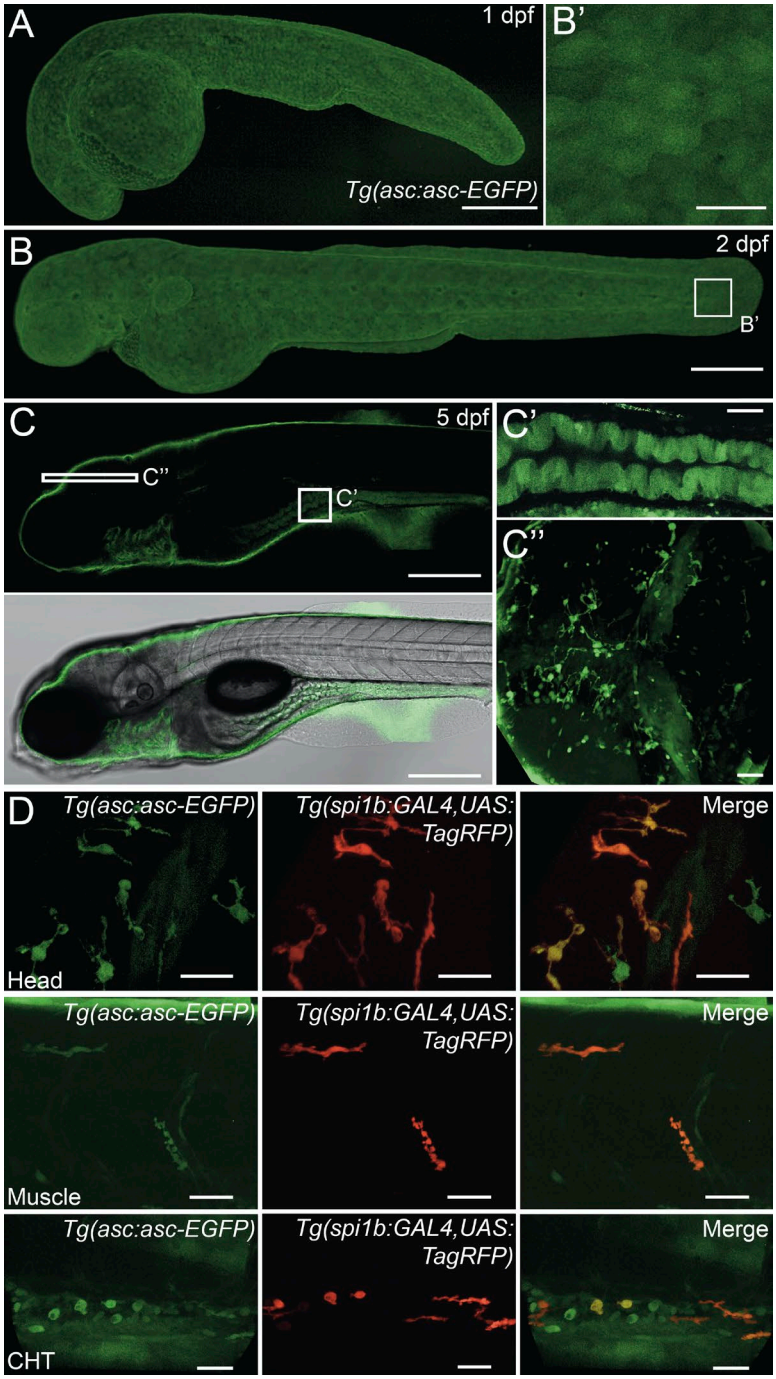

Figure 2. **Endogenous ASC visualized in vivo in the *Tg(asc:asc-EGFP)* line.** Live imaging of *Tg(asc:asc-EGFP)* for 1-dpf (A), 2-dpf (B), and 5-dpf (C) larvae, with magnification of skin (B′), intestine (C′), and head (C″) optical sections. Live imaging of head, muscle, and caudal hematopoietic tissue (CHT) of 3-dpf *Tg(asc:asc-EGFP, spi1b:GAL4,UAS:TagRFP)* larvae (D). Bars: (full larvae) 300 µm; (all others) 30 µm.

HSE:asc-mKate2, in which mKate2-tagged ASC was expressed under the control of a heat-shock promoter, which allowed us to induce ASC expression throughout the fish, including cells that do not express it endogenously. Transient expression of ASC–mKate2 from this construct led to the appearance of specks, whereas mKate2 alone had a cytoplasmic distribution (Fig. S2 A). Speck formation was not caused by the mKate2 fused to the ASC or by heat-shock–related stress because overexpressing ASC with other tags and using other expression systems also resulted in speck formation (Fig. S3, B–E). To simultaneously and stably induce ASC–mKate2 overexpression in all cells, we generated the transgenic line *Tg(HSE:asc-mKate2)* (Fig. 4 B). A quantification of speck formation over time in transgenic embryos showed that, from 2.5 h post–heat shock (hphs), the number of specks increases rapidly, and then, plateaus at around 17 hphs (Fig. 4 C and Video 3). Each cell formed only one speck, concomitant with the depletion of the cytoplasmic pool of ASC–mKate2 (Fig. 4 D and Video 3). Although muscle cells do not express *asc* endogenously, the heat-shock–induced ASC–mKate2 also assembled into a single speck in these cells. When we overexpressed ASC–mKate2 in *Tg(asc:asc-EGFP)* embryos, specks that formed in muscle cells were constituted exclusively by ASC–mKate2 (Fig. 4 E), whereas in epidermal cells, the endogenous ASC–GFP was recruited to the ASC–mKate2 speck (Fig. 4 F and Video 2). These results suggest that overexpression of ASC or its upstream receptors trigger speck formation and bypass the need for an inflammatory stimulus to activate inflammasome signaling.

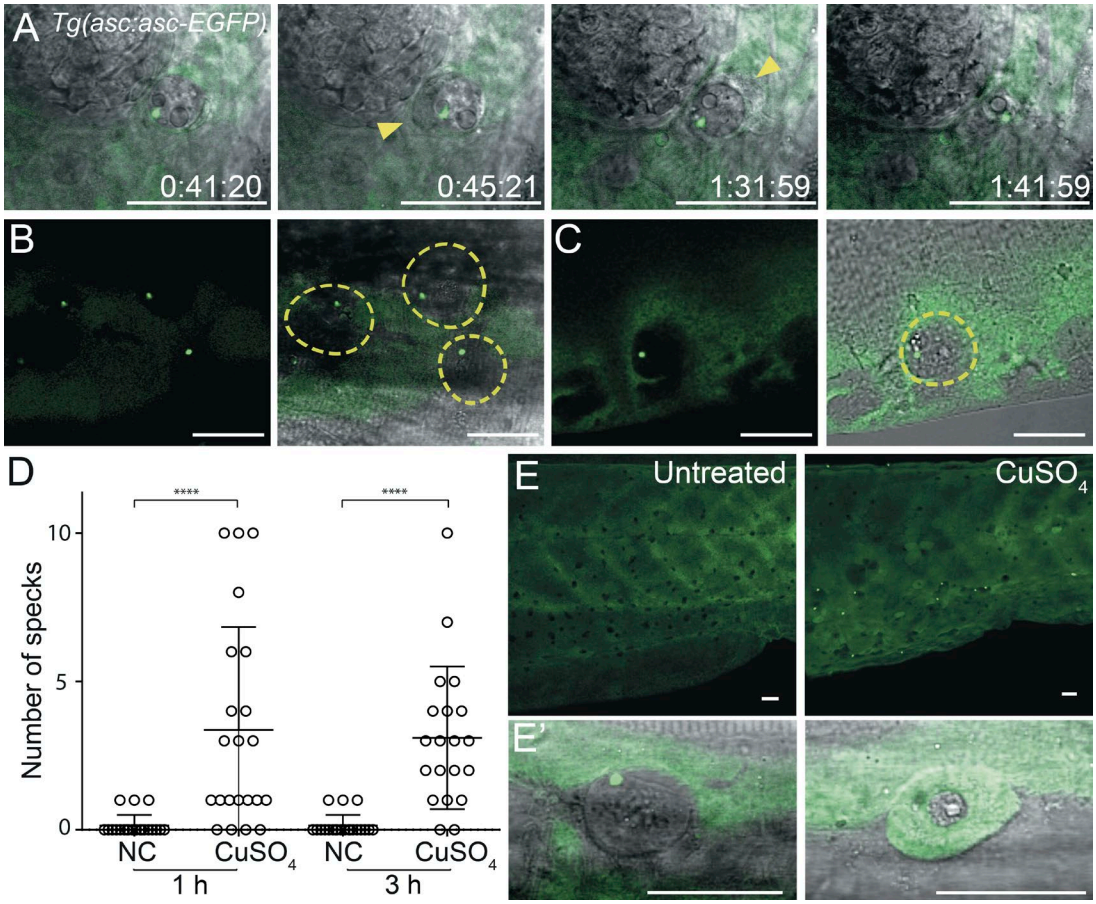

Figure 3. **Live imaging of endogenous speck formation in the *Tg(asc:asc-EGFP)* line.** Time-lapse imaging of a keratinocyte with a speck. Single plane merged with the brightfield is shown. (A) Yellow arrowheads highlight a second cell that appears to surround the speck-containing cell. Full time-lapse is included in Video 1. Live imaging of specks in the dorsal epidermis (B) and ventral fin (C) of 3-dpf *Tg(asc:asc-EGFP)* larvae. Merge with brightfield plane shows each speck is within a cell with altered morphology (dashed yellow line). (D) *Tg(asc:asc-EGFP)* 3-dpf larvae were treated with 25 µM $CuSO_4$ for 1 h. At 1 and 3 h after treatment, the number of specks per larva were quantified (one-way ANOVA; ****, $P < 0.0001$). Live imaging of untreated and treated larvae showing high damage of epidermis and increase in specks (E), examples in treated embryo of single cells displaying altered morphology with and without speck formation (E'). Bars: (full larvae) 300 µm; (all others) 30 µm.

Specks are formed by large, filamentous assemblies of ASC

Based on cryo-EM structures of in vitro–assembled PYD_A filaments and EM data of ASC specks reconstituted in vitro (Lu et al., 2014), specks are thought to be composed of cross-linked filaments that aggregate into a sphere (Lu and Wu, 2015). To characterize the structure of in vivo–formed specks, we used correlative light and electron microscopy (CLEM; Fig. 5, A and B). We visualized ultrastructural details of specks formed in muscle cells after inducing ASC–mKate2 expression in the *Tg(HSE:asc-mKate2)* line. Specks in muscle cells form a cluster of 700 nm in diameter, consisting of highly intercrossed filaments (Fig. 5 B and Video 4). A three-dimensional model of the filaments reveals that the aggregated ASC filaments form a globular structure (Fig. 5 C and Video 4). These data are a strong indication that the filamentous organization observed from in vitro studies is also true of in vivo, assembled specks.

Mutating conserved, predicted phosphorylation sites abrogates speck formation

Activation of ASC, similar to other inflammasome components, is subjected to regulation by posttranslational modifications (Hoss et al., 2017). Thus, the speck formation we observed should depend on those modifications as well. We used the overexpression system to test whether ASC in zebrafish was regulated through phosphorylation by the JNK and spleen tyrosine kinase (Syk) signaling pathways, as reported for mammalian ASC (Hara et al., 2013; Lin et al., 2015). An in silico analysis, as used by Hara et al. (2013), predicted several potential JNK and Syk phosphorylation sites in zebrafish ASC (Table S1). Three sites corresponded to residues within the $CARD_A$ that are conserved in mouse and human ASC (Fig. 5 D and Fig. S2 F). We mutated those three sites (Y152F, T160F, and T170A) and one additional site in PYD_A, which was not conserved (T38A). Because muscle cells do not express *asc* endogenously, we were able to use these cells for an in vivo analysis of speck formation by mutant proteins and avoid interference from the WT ASC. Transiently expressed ASC–mKate2, containing the four mutations, formed a striated pattern or large, filamentous aggregates in muscle cells, rather than a compact speck (Fig. 5 E). By expressing constructs with single mutations, we found that the Y152F mutation was sufficient to disrupt the speck formation entirely (Fig. 5 F), similar to the corresponding mutations in mouse (Y144A) or human (Y146A) ASC, which also caused defective speck formation

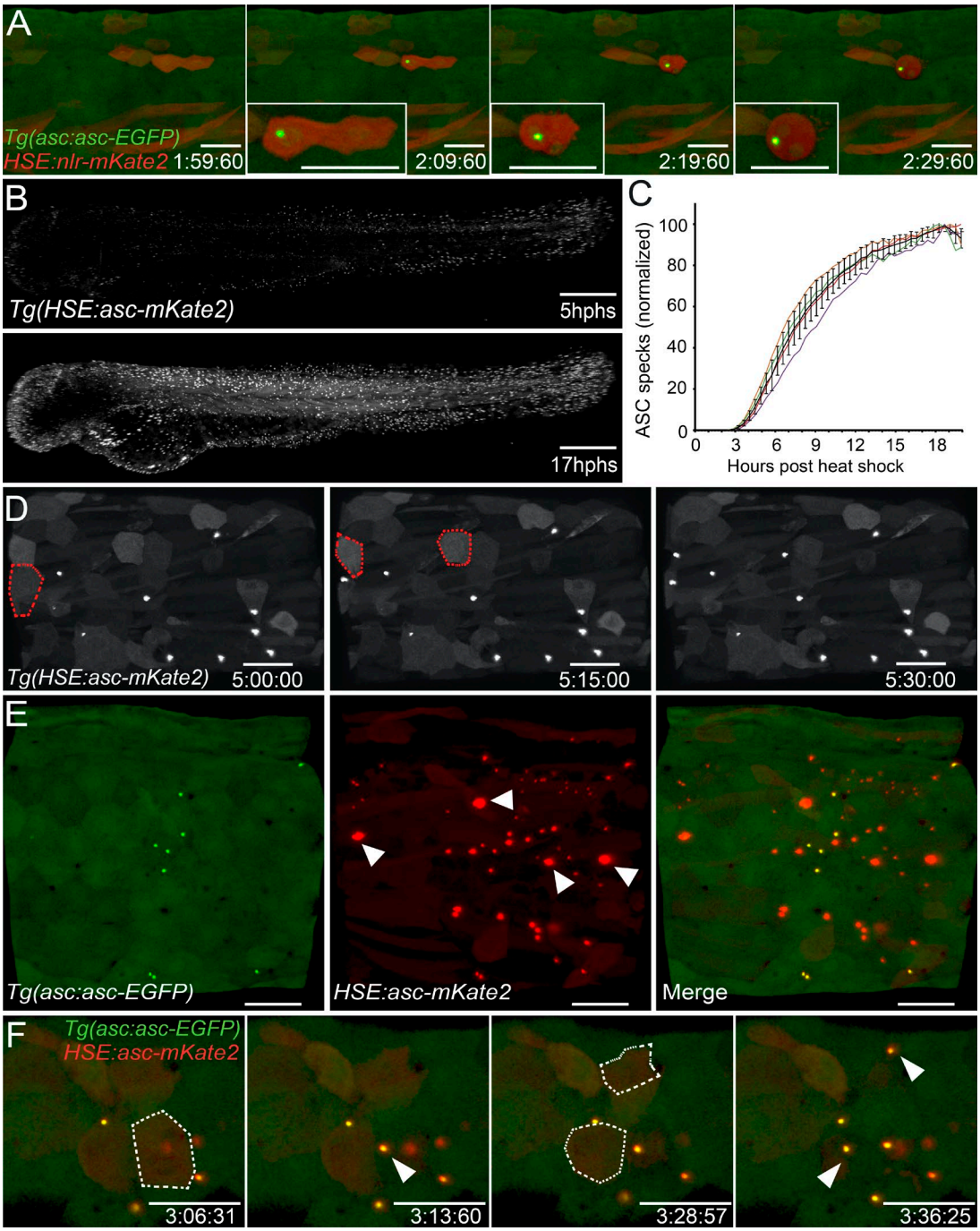

Figure 4. **Expression of ASC or NLR induces speck formation.** Time-lapse imaging of trunk from 3-dpf *Tg(asc:asc-gfp)* larva transiently expressing *HSE:nlr-mKate2* at 7 hphs. (A) Inset shows enlarged view of NLR-mkate2–expressing keratinocytes after speck formation. Full time-lapse is included in Video 2. (B) Time-lapse imaging of 3-dpf *Tg(HSE:asc-mKate2)* embryos after heat shock. Shown are time points corresponding to 5 hphs (top) and 17 hphs (bottom). (C) Quantification of speck numbers over the entire larvae in five samples imaged overnight after heat shock using three-dimensional image analysis software. (D) Time-lapse of 3 dpf *Tg(HSE:asc-mKate2)* larvae 3 hphs showing recruitment of ASC-mKate2 to a single speck per cell (demarcated by dashed red line at the time point before speck formation). Both *Tg(HSE:asc-mKate2)* larvae time-lapses are included in Video 3. (E) Live imaging of *Tg(asc:asc-gfp)* transiently expressing *HSE:asc-mKate2* at 13 hphs. White arrowheads show specks assembled in muscles. (F) Time-lapse imaging of *Tg(asc:asc-gfp)* larva transiently expressing *HSE:asc-mKate2*. Individual keratinocytes are demarcated with a dashed white line at the time point before the formation of ASC–mKate2 and ASC–GFP double-positive specks (white arrowheads). Time-lapse was started 3.5 hphs. Full time-lapse is included in Video 3. Bars: (full larvae) 300 µm; (all others) 40 µm.

(Hara et al., 2013; Lin et al., 2015). These results support the notion that speck formation caused by the experimental conditions used here is under the control of conserved ASC post-translational regulatory mechanisms, and assembly, therefore, follows the physiologic signaling pathway.

Speck formation leads to keratinocyte pyroptosis

It is well established that speck formation can cause cell death by macrophage pyroptosis in culture. However, the first barrier a pathogen must overcome to establish infection is the epithelial

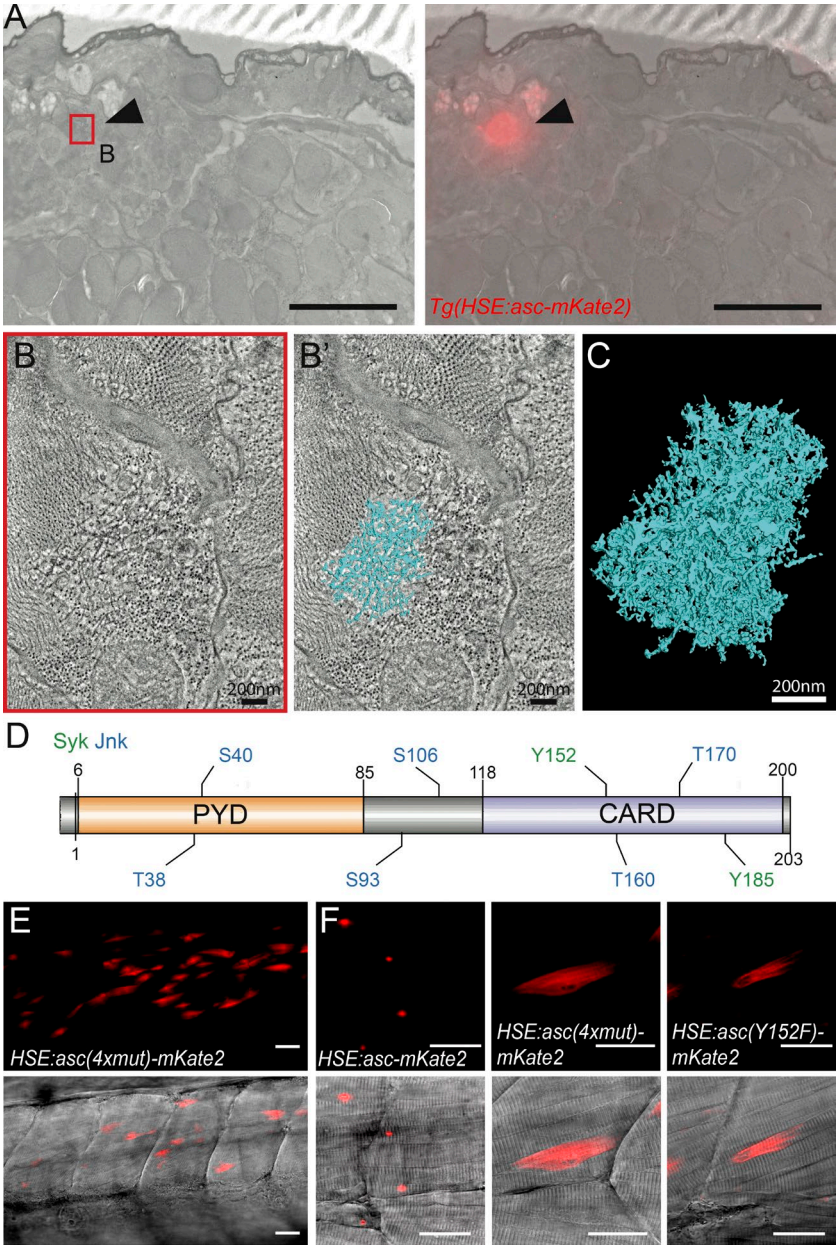

Figure 5. **ASC specks are highly intercrossed, filamentous structures whose clustering is altered by point mutations.** (A–C) CLEM of high-pressure frozen 3 dpf *Tg(HSE:asc-mKate2)* larvae at 18 hphs. Low magnification electron micrograph (A, left) and overlay with red channel (A, right) imaged with light microscope. Black arrowhead shows location of speck. (B) Area of interest (red box) imaged with electron microscope. TEM tomography slice of the speck (B, black arrowhead) and overlay with 3D reconstruction of speck after manual tracking of individual filaments (B′). (C) Zoom in of three-dimensional reconstruction model. Entire TEM tomography stack and three-dimensional model are found in Video 4. Bars, 10 µm, unless otherwise indicated. (D) Results from phosphorylation-site analysis using the online tool GPS version 2.1.1, depicting Syk and JNK-specific, predicted phosphorylation sites in zebrafish ASC. Full results are found in Table S1. (E) Live imaging of larvae transiently expressing *HSE:asc(4xmut)-mKate2*, containing four missense mutations (T38A, Y152F, T160A, and T170A). (F) Single muscle cell in larvae transiently expressing either *HSE:asc-mKate2*, or *HSE:asc(4xmut)-mKate2*, or *HSE:asc(Y152F)-mKate2*. Bars, 30 µm.

surfaces that cover the body, which, as we have shown, express high levels of ASC. In spite of this, very little is known about the function and dynamics of ASC activation and speck formation in this important tissue. Because inducing *asc* expression in the *Tg(HSE:asc-mKate2)* line allowed us to study cell type–specific responses to speck formation, we compared responses of keratinocytes, which endogenously express *asc*, to muscle cells, which do not. We observed starkly different responses to speck formation. Keratinocytes round up within minutes after speck formation, whereas muscle cells show no visible change over ≥10 h; during which, the speck continuously increases in size (Fig. 6 A and Video 5). The response in epidermal cells was independent of the method used to overexpress ASC (Fig. S2 G). That the appearance of ASC–mKate2 specks is associated with the same morphological changes as those seen after the formation of endogenous ASC–GFP specks suggests that inflammasome signaling is being activated in these cells as a result of overexpression-induced speck formation.

We quantified cell death in the *Tg(HSE:asc-mKate2)* line with acridine orange (Fig. 6 B). Before specks assemble, *Tg(HSE:asc-mKate2)* and control larvae show similar levels of staining. However, after speck formation, cell death was significantly higher in heat-shocked, transgenic larvae (Fig. 6 C). Most of the acridine orange staining was located in the skin (Fig. S2 H); and keratinocytes, but not muscle cells, accumulated acridine orange in their surroundings after speck formation (Fig. S2 I). This, together with the observed changes in morphology, suggested that keratinocytes were undergoing cell death upon speck formation. To test that, we monitored the cellular changes in response to speck formation, specifically in EVL keratinocytes, using *Tg(krt4:GFP, HSE:asc-mKate2)* larvae (Fig. 6 D and Video 5). All GFP$^+$ cells that formed a speck showed classic signs of pyroptosis (Vande Walle and Lamkanfi, 2016) <15 min after speck formation, including rounding up, detachment from the epithelia, and loss of plasma membrane integrity. We analyzed the process of cell extrusion by

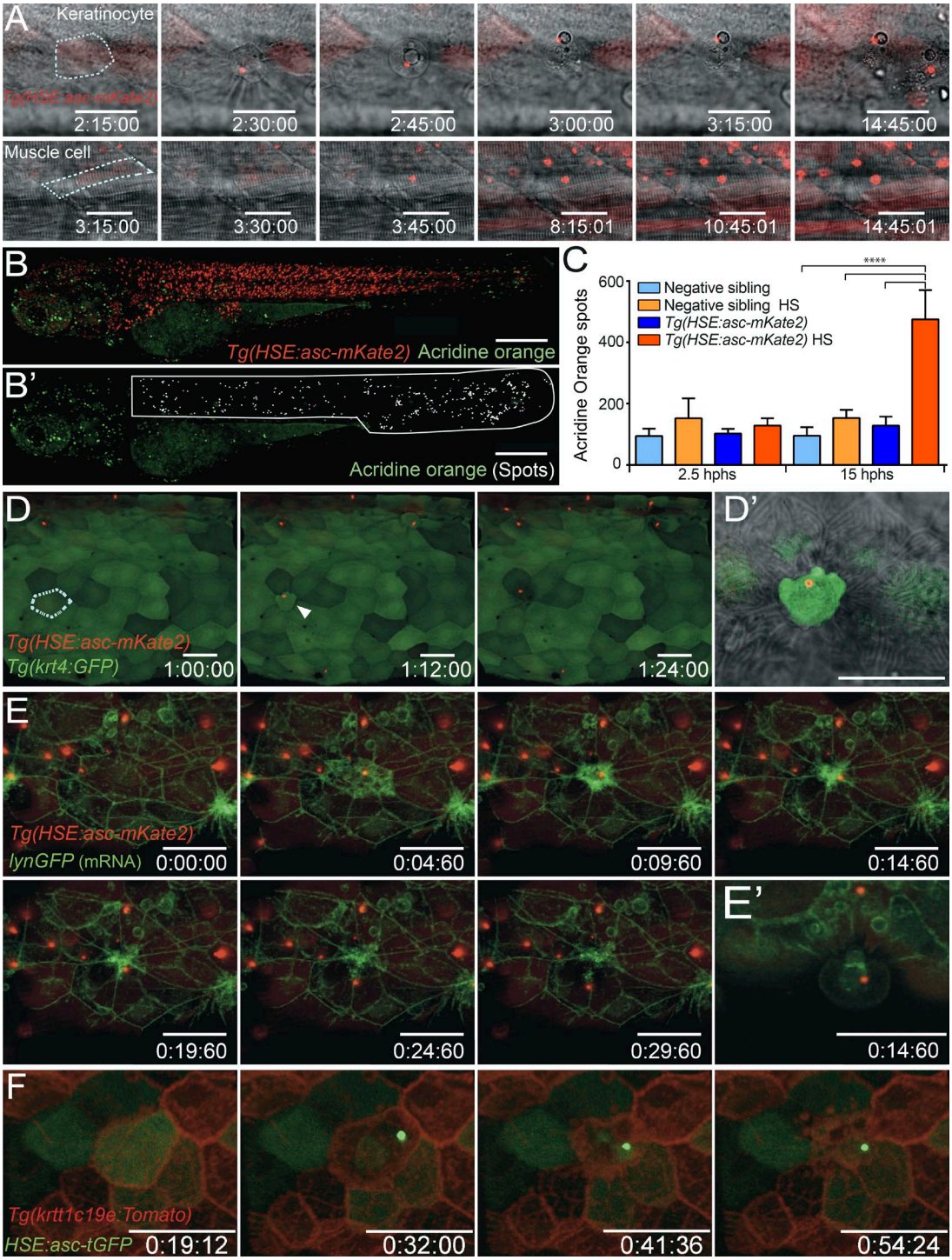

Figure 6. **ASC speck formation in keratinocytes leads to cell death.** (A) Time-lapse imaging of speck formation in keratinocyte (top) and muscle cell (bottom) in 3 dpf *Tg(HSE:asc-mKate2)* larva at 3 hphs. (B) Drastic, morphological changes occur only in keratinocytes. *Tg(HSE:asc-mKate2)* larvae, and negative siblings were stained with acridine orange and imaged at 2.5 and 15 hphs. 3D rendering of individual larvae manually segmented to exclude the head, heart and yolk regions. (B′) Acridine orange spots in segmented region were quantified using 3D image analysis software (white spots); spots positive in the red channel were excluded (magenta spots). (C) Histogram of acridine orange spots in each group shows only transgenic larvae at 15 hphs have significantly higher cell death (one-way ANOVA; ****, $P < 0.0001$). (D) Time-lapse imaging of *Tg(HSE:asc-mKate2, krt4:GFP)* larvae at 3 hphs showing morphological changes in EVL keratinocyte upon speck formation (white arrowhead). Enlarged view of EVL keratinocyte (dashed white outline) of single plane with the brightfield (D′). (E) Time-lapse imaging of *Tg(HSE:asc-mKate2)* injected with *lynGFP* mRNA for membrane visualization at 8 hphs. Epidermal layer shows extrusion and gap closure after speck formation. (E′) Single plane showing extruded keratinocyte. (F) Time-lapse imaging of 3-dpf *Tg(krtt1c19e:Tomato)* larva transiently expressing *HSE:asc-tGFP*, showing plasma membrane collapse and cell extrusion after speck formation in keratinocytes. All time-lapses are included in Video 5. Bars, 30 µm.

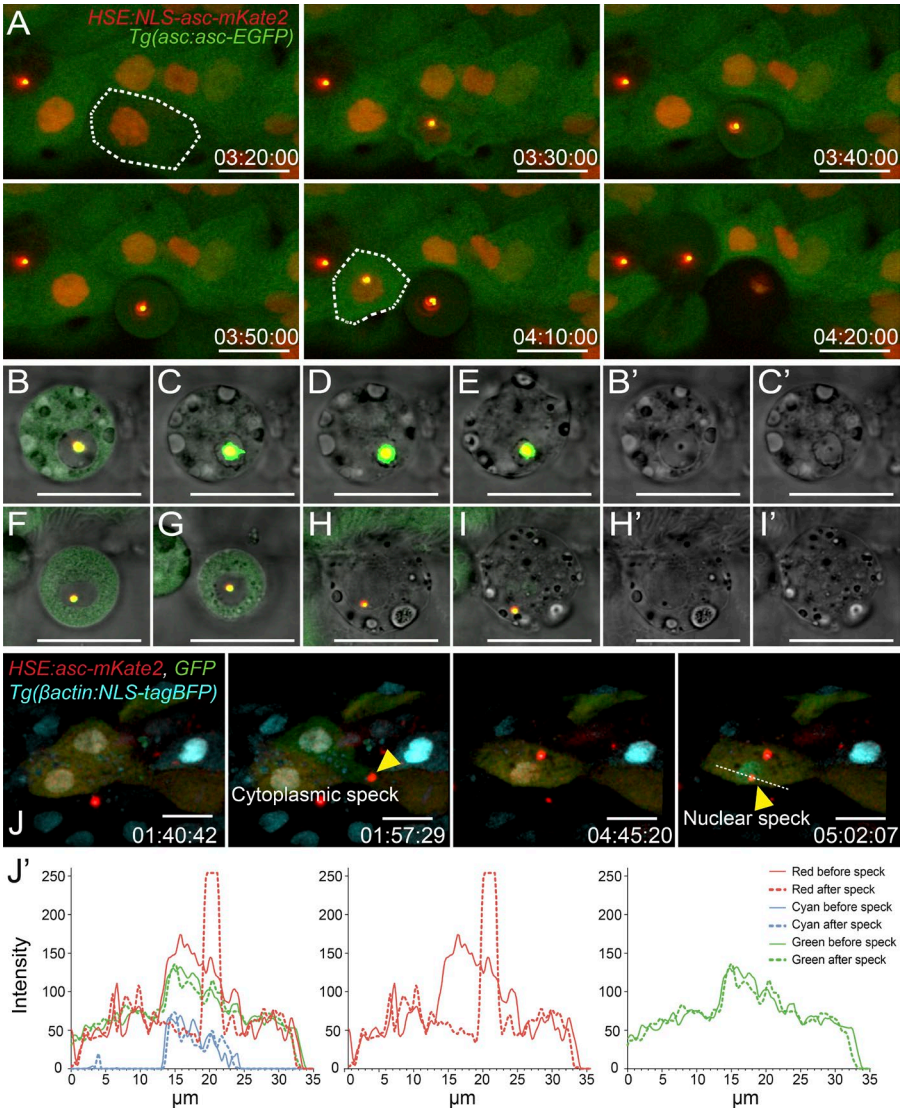

Figure 7. **Speck formation in the nucleus causes cell death.** (A) Time-lapse of 3-dpf *Tg(asc:asc-EGFP)* larvae transiently expressing *HSE:NLS-asc-mKate2* at 6 hphs, showing that nuclear speck assembly in keratinocytes (white dashed line) leads to cell death. (B–E) Cell undergoing cell death with nuclear speck and without depletion of ASC–GFP in the cytoplasm. Brightfield of respective time points show breakdown of nuclear envelope, allowing recruitment of cytoplasmic ASC–GFP (B′ and C′). Loss of plasma membrane integrity (F–I) before nuclear envelope breakdown, results in leakage of cytoplasmic ASC–GFP as shown in brightfield (H′ and I′). (J) Time-lapse imaging of transient ASC–mKate2 and GFP expression in *Tg(βactin:NLS-tagBFP)* larvae at 6 hphs. Yellow arrowheads signal speck formation events in two adjacent cells; first, within the cytoplasm, and second, within the nucleus. (J′) Intensity plot profile (white dashed line) before and after nuclear speck formation for all channels. (Middle and right) Green and red channels shown separately, highlighting ASC–mKate2 depletion only from nuclear pool. Full time-lapses are included in Video 6. Bars, 20 µm.

labeling the plasma membrane with a membrane-targeted GFP (lynGFP) and observed that speck formation led to extrusion of the pyroptotic cell from the epithelial sheet, with surrounding cells sealing the gap (Fig. 6 E and Video 5). This was also seen after transient overexpression of ASC–turbo-GFP (tGFP) in a reporter line labeling the membranes of keratinocytes (Fig. 6 F and Video 5). These results show that keratinocytes undergo pyroptosis within 15 min of speck formation.

Effect of speck formation by nuclear ASC

Both when detected by antibodies and when tagged by GFP, endogenous ASC is present in the cytoplasm and the nucleus. Either pool can form specks in HeLa cells (Cheng et al., 2010), although the significance of that and, in particular, whether both nuclear and cytoplasmic specks can induce cell death in vivo, is unclear. To test that, we transiently expressed a nuclear-targeted ASC–mKate2 (NLS-ASC-mKate2) in the *Tg(asc:asc-EGFP)* line, which allowed us to monitor not only the effect of nuclear ASC but also the endogenous nuclear and cytoplasmic ASC pools. When NLS-ASC-mKate2 formed specks in the nucleus of ASC–GFP-expressing keratinocytes, those cells underwent cell death with the same dynamics as described for keratinocytes overexpressing ASC-mKate2 (Fig. 6). Cell death occurred without the recruitment of the cytoplasmic pool of the endogenous ASC–GFP (Fig. 7 A and Video 6). Therefore, the presence of a nuclear speck is sufficient, and neither the depletion of the cytoplasmic pool nor a cytoplasmic speck is required for keratinocyte pyroptosis. However, in cases in which the nuclear envelope became permeable to the endogenous ASC–GFP before death occurred, the cytoplasmic pool of ASC–GFP was also recruited to the nuclear speck (Fig. 7, B–E). In cases in which the plasma membrane collapsed before the nuclear-envelope breakdown, cytoplasmic ASC–GFP leaked to the extracellular environment before it was recruited to the nuclear speck (Fig. 7, F–I). From 50 cells in 17 larvae from three biological replicates, we observed 27 cases in which the cytoplasmic GFP was lost and 23 in which it was recruited to the speck. We again observed nuclear speck formation by transiently coexpressing ASC–mKate2 with GFP in a transgenic line carrying the *βactinNLS-tagBFP* transgene to label all nuclei (Fig. 7 J and Video 6). Specks assembled from either the cytoplasmic or the nuclear pools of ASC, but regardless of the compartment in which the speck formed, its assembly led to cell death. This confirms that speck formation in the nucleus is sufficient to trigger pyroptosis in keratinocytes.

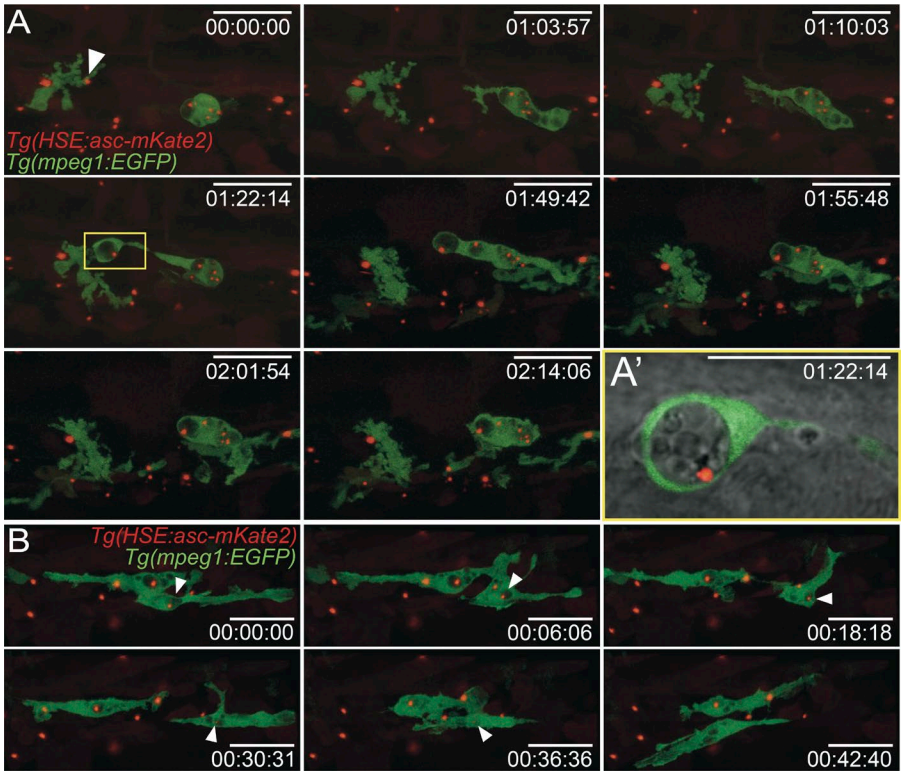

Figure 8. **Macrophage engulfment of speck-containing pyroptotic debris.** (A) Time-lapse imaging of *Tg(HSE:asc-mKate2, mpeg1:EGFP)* larva at 17 hphs shows macrophage engulfing a speck (white arrowhead). (A′) Enlarged view of single plane with brightfield merge showing phagocytic cup (boxed in yellow). (B) Second time-lapse imaging of *Tg(HSE:asc-mKate2, mpeg1:EGFP)* larvae at 17 hphs, showing degradation of speck within phagosome (white arrowhead). Full time-lapses are included in Video 7. Bars, 30 µm.

Clearance by macrophages of pyroptotic debris containing ASC specks

After macrophages undergo pyroptosis, they leave behind a structure composed of ruptured plasma membrane containing insoluble contents called "pore-induced intracellular traps" (PITs). In culture, neighboring phagocytes clear up PITs through efferocytosis (Jorgensen et al., 2016). There is also evidence that ASC specks are released to the extracellular space and can spread inflammation by recruiting the soluble ASC in the cytoplasm of phagocytes that engulf them (Baroja-Mazo et al., 2014; Franklin et al., 2014). However, whether ASC specks remain trapped in PITs and the rules that determine when engulfed specks induce speck formation and pyroptosis in the phagocyte have yet to be defined. We observed that, after keratinocyte cell death, specks remained enclosed within the cellular debris (Fig. 3, A–C; and Fig. 6 A). To test whether phagocytes could engulf speck-containing cellular debris, we induced ASC–mKate2 expression in the *Tg(HSE:asc-mKate2)* line, crossed with the macrophage reporter line. Macrophages were indeed capable of engulfing pyroptotic debris with specks (Fig. 8 A and Video 7). Instances of macrophages containing multiple phagosomes with specks suggest there is continuous uptake of speck-containing debris by phagocytes and that engulfed specks do not elicit a pyroptotic response in the macrophages within 2–3 h after engulfment. Instead, the gradual loss of fluorescence from phagocytized ASC–mKate2 specks suggests that macrophages are capable of digesting specks after engulfment (Fig. 8 B and Video 7). To test whether macrophages themselves form specks during this process, we visualized the engulfment and digestion of specks by inducing the transient expression of ASC–mKate2 in the *Tg(asc:asc-EGFP)* line, crossed with a line with macrophages carrying a red membrane label. Macrophages digested the engulfed specks, but their endogenous ASC–GFP remained distributed throughout the cytoplasm during that process (Video 7). Thus, the main function of phagocytes that we observed in vivo is to clear speck-containing, pyroptotic cellular debris, and we have seen no incidences of specks triggering further death after engulfment.

Domain requirements for compact speck clustering and efficient cell death

Based on in vitro and cell culture experiments, the PYD and CARD domains of ASC are thought to have distinct roles during speck formation, with PYD_A assembling into filaments that are cross-linked by interfilament CARD interactions (Dick et al., 2016). To determine each domain's role in speck assembly and pyroptosis in vivo, we overexpressed the single PYD_A and $CARD_A$ fused to mKate2 (PYD_A–mKate2 and $CARD_A$–mKate2, respectively). In muscle cells, PYD_A most frequently assembled into long, filamentous structures, whereas $CARD_A$ aggregated into smaller punctate aggregates throughout the cell (Fig. 9 A). In contrast, expression of either domain keratinocytes resulted in the formation of a normal-looking, compact speck, which led to pyroptosis (Fig. S3, A and B; and Video 8). The most likely reason for this difference is the presence of endogenous ASC in keratinocytes. To test that, we repeated those experiments under conditions of *asc* morpholino knockdown (Fig. S3 C). Although overexpressed ASC*–mKate2 (*asc* morpholino-resistant) under *asc* knockdown conditions formed compact specks in keratinocytes and caused cell death (Fig. S3 D and Video 8), as observed in control larvae, overexpressed PYD^*_A or $CARD_A$ failed to do so. Instead, after a slower depletion of the cytoplasmic pool of the protein than that of full-length ASC, the single domains formed aggregates similar to those assembled in muscle cells (Fig. 9, B and C; and Video 8). The formation of these aggregates was not associated with immediate cell death: PYD_A-expressing epidermal cells died over

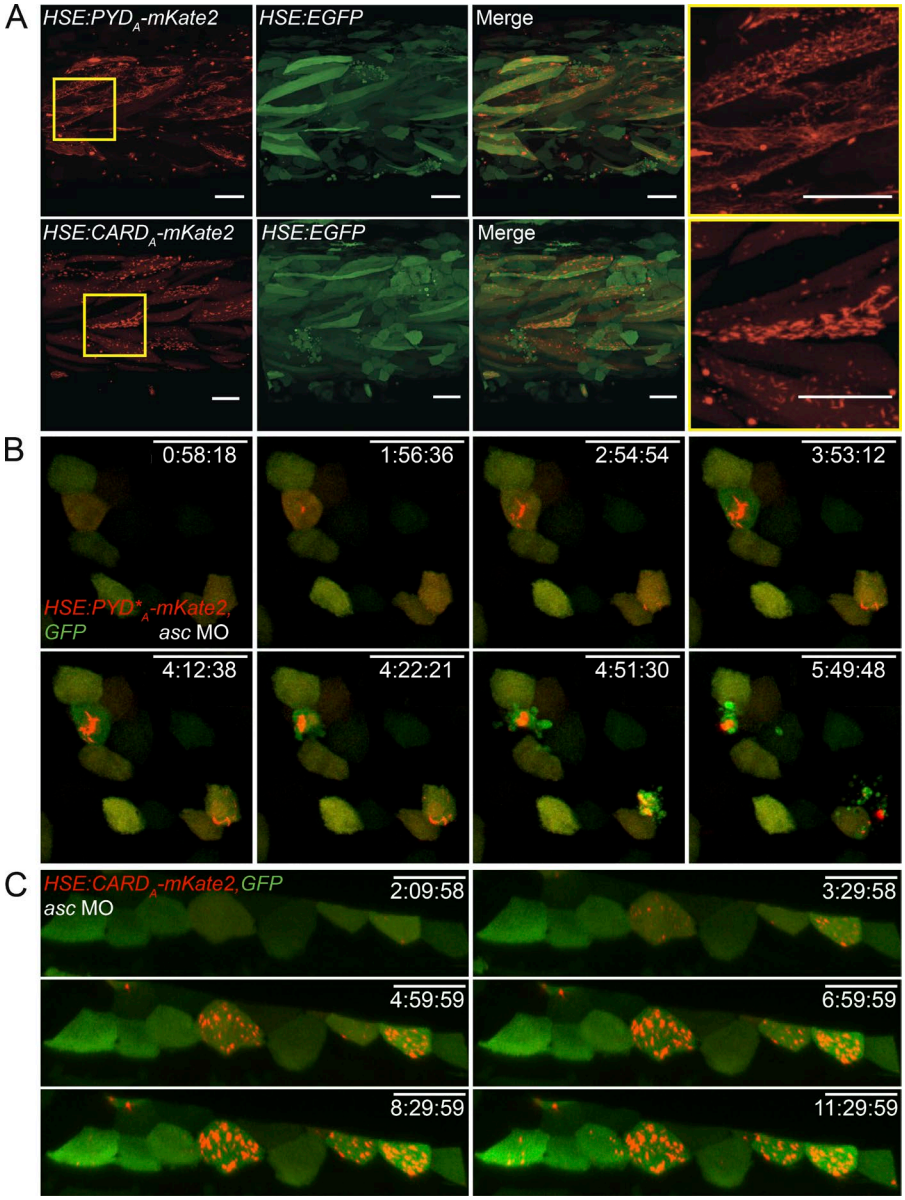

Figure 9. **PYD aggregates lead to delayed pyroptosis.** (A) Live imaging of 3-dpf larvae transiently expressing *HSE:PYD$_A$-mKate2* or *HSE:CARD$_A$-mKate2* with GFP at 17 hphs. Expression of either domain leads to the formation of filamentous aggregates of varying lengths in muscle cells. Time-lapse imaging of *asc* morpholino-injected *Tg(asc :asc-EGFP)* larvae transiently expressing the *asc* morpholino-resistant *HSE:PYD*$^*_A$–mKate2* (B) or *HSE:CARD$_A$–mKate2* (C) with GFP. If endogenous ASC is absent, PYD*$_A$ aggregates cause cell death 2 h after the aggregates first form, whereas CARD$_A$ aggregates do not, even at 10 h after their assembly. Full time-lapses are included in Video 8. Bars, 40 µm.

2 h after PYD$_A$ aggregates were first seen, whereas cells with CARD$_A$ aggregates survived for >10 h after aggregate formation. This differs from the fast response observed within ∼10 min of ASC–mKate2 speck formation in *asc* knockdown larvae. PYD$_A$ is, therefore, both necessary and sufficient for cell death, which suggests that this domain mediates the interaction with downstream elements that trigger pyroptosis.

PYD-dependent recruitment of Caspa to the ASC speck

In mammals, the effector domain of ASC for triggering pyroptosis is the CARD, which interacts with the CARD of Caspase-1. For that reason, it is surprising that, in zebrafish, PYD appears to be the effector domain. We, therefore, tested whether caspases were involved in the response to speck formation, and if so, how they interacted with ASC. Treatment of *Tg(HSE:asc-mKate2)* larvae with the pan-caspase inhibitor (Q-VD-OPh hydrate) resulted in a significant reduction in cell death, without affecting speck formation (Fig. 10, A and B), showing that caspase activity is required for ASC-dependent pyroptosis. Because caspases are recruited to the speck for autoactivation (Man and Kanneganti, 2016), we tested which caspases could interact with the ASC speck. There are two homologues of mammalian *caspase-1* in zebrafish, *caspa* and *caspb*, both with N-terminal PYD domains. We generated GFP fusions for both caspases, as well as for *casp3a*, the zebrafish orthologue of mammalian Caspase-3, and transiently coexpressed them with ASC–mKate2. Only Caspa was recruited to ASC specks assembled in muscle cells (Fig. 10 C). By expressing the PYD and p20–p10 domains of Caspa (PYD$_C$ and p20–p10) separately with either the PYD$_A$ or CARD$_A$, we confirmed that the interaction occurs via the PYD domains of both proteins (Fig. 10 D and Fig. S4, A–C).

Transient overexpression of Caspa, unlike that of Caspb or Casp3a, was extremely toxic to epidermal cells (Fig. 10 E). Caspa–GFP-overexpressing embryos lacked normal-looking keratinocytes with homogeneous GFP expression and, instead, had copious green-labeled cellular debris. Even muscle cells, which were not affected by ASC speck formation, displayed signs of damage after Caspa expression (Fig. 10 F). Consider-

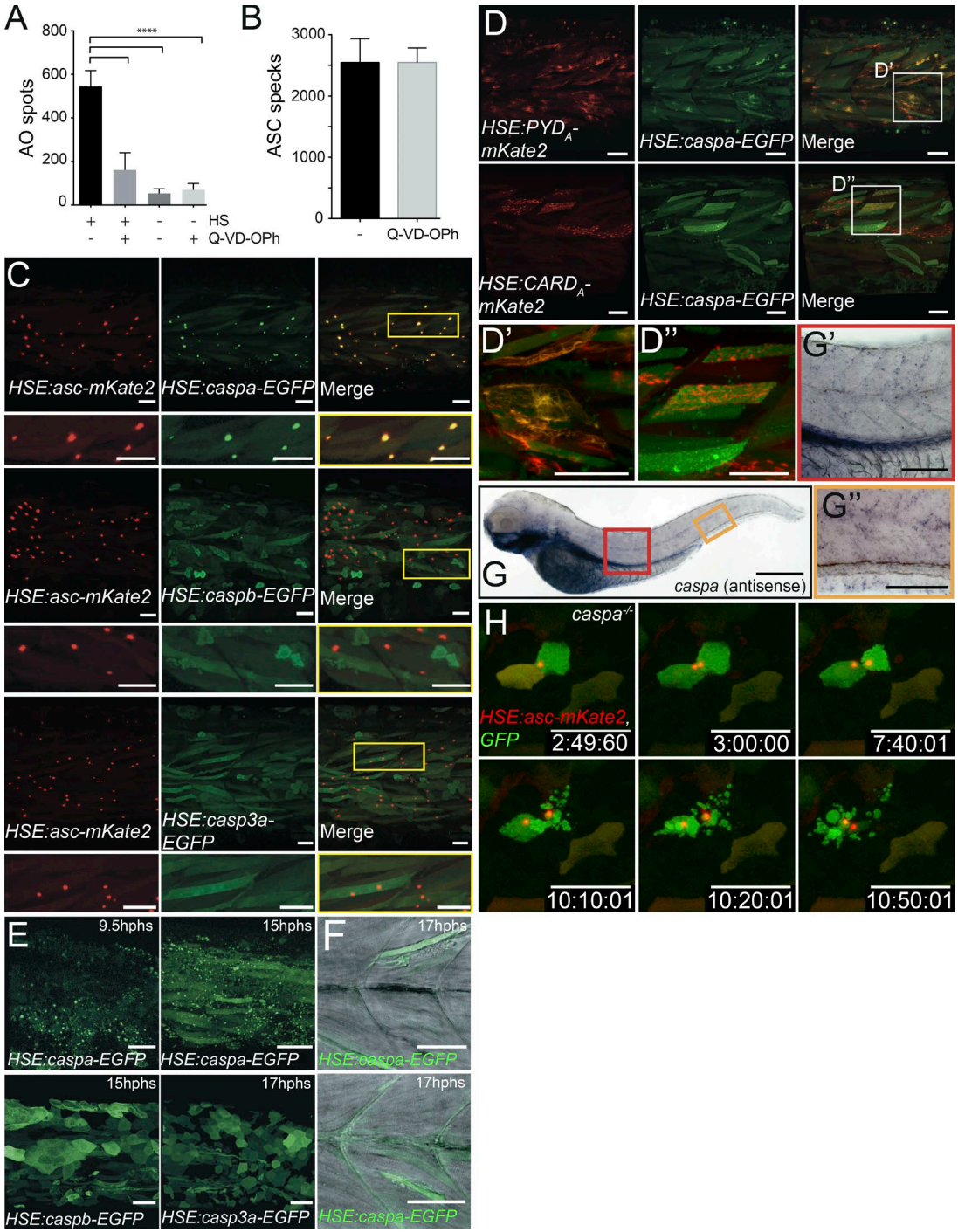

Figure 10. **ASC speck formation leads to pyroptosis via activation of Caspa through PYD–PYD domain interaction.** 3-dpf *Tg(HSE:asc-mKate2)* larvae treated with the pan-caspase inhibitor Q-VD-Oph (100 µM) after or without heat shock were stained with acridine orange at 17 hphs. Acridine orange (AO) spots (A) and specks (B) were quantified. Treatment with Q-VD-Oph significantly diminished cell death caused by speck formation compared with nontreated controls (one-way ANOVA; ****, $P < 0.0001$) but did not affect speck formation. (C) Live imaging of transient expression of *HSE:caspa-EGFP*, *HSE:caspb-EGFP*, or *HSE:casp3a-EGFP* with *HSE:asc-mKate2*. Recruitment to the ASC–mKate2 specks only occurs in the case of Caspa–GFP coexpression. Enlarged view of single muscle cells for each case (yellow boxes) are shown below their corresponding row. Live imaging of heat-shock–induced transient expression of *HSE:PYD$_A$-mKate2* or *HSE:CARD$_A$-mKate2* with *HSE:caspa-EGFP* in 3-dpf larvae at 19 hphs (D) with enlarged view of single cells (D′ and D″). (E) PYD$_A$, but not CARD$_A$, aggregates recruit Caspa-GFP. Live imaging of transient expression of *HSE:caspa-EGFP*, *HSE:caspb-EGFP*, or *HSE:casp3a-EGFP* between 9 and 17 hphs. Vast amounts of epidermal cellular debris are seen only when Caspa–GFP is overexpressed. (F) Single plane of *HSE:caspa-EGFP* transient expression at 17 hphs in muscle cells showing morphological changes upon Caspa–GFP overexpression. *caspa* antisense *wish* in 3-dpf larvae (G). Enlarged view shows expression in skin (G′) and ventral fin (G″). (H) Time-lapse imaging of *caspa* mutants transiently expressing *HSE:asc-mKate2* with GFP at 3 hphs. Cell death response is severely affected in *caspa*$^{-/-}$ keratinocytes, with cells dying an apoptotic-like death >7 h after speck formation. Full time-lapses are included in Video 9. Bars: (full larvae) 300 µm; (all others) 40 µm.

ing that endogenous *caspa* is expressed in the skin (Fig. 10 G and Fig. S4 D), these data strongly suggest that Caspa is the effector caspase that activates pyroptosis in keratinocytes after speck formation and that muscle cells are protected from speck-induced pyroptosis because they do not express it.

To test that hypothesis, we generated a *caspa* mutant with CRISPR/Cas9 and identified two mutations (*caspa*^{K**} and *caspa*$^{\Delta 800}$), which resulted in transcripts with a nonsense codon within the first exon (Fig. S4, E–G). We transiently expressed ASC–mKate2 and GFP in *caspa* knockout larvae. Speck formation in keratinocytes proceeded normally in those larvae but did not result in pyroptosis, with cells, instead, surviving for hours after speck formation (Fig. 10 H and Video 9). Eventually, keratinocytes with specks displayed cellular blebbing, nuclear condensation, and slowly disintegrated into vesicles strongly reminiscent of apoptotic bodies, suggesting that if Caspa is absent, speck formation results in activation of apoptosis instead of pyroptosis.

Caspase-8–dependant apoptotic death can occur downstream of speck formation via heterotypic PYD/DED interaction in the absence of Caspase-1 (Vajjhala et al., 2015). We found that, like Caspa–GFP, transient overexpression of the zebrafish Caspase-8 orthologue (Casp8) was highly toxic to cells (Fig. S4 H). These results establish Caspa as the direct and only downstream effector of ASC speck formation driving immediate pyroptosis in vivo.

Discussion

ASC speck formation is a hallmark of inflammasome activation. The use of cell lines has significantly contributed to dissect the molecular interactions involved in this signaling cascade, but we lack deeper understanding of how inflammasome activation occurs in cells within their native environment. This knowledge gap can be bridged by using models that enable visualization of immune processes in the context of the whole organism (Renshaw and Trede, 2012; Lin et al., 2016). Previous studies had suggested that some elements of the inflammasome signaling cascade are involved in the defense against pathogens using zebrafish infection models (Vojtech et al., 2012; Varela et al., 2014; Vincent et al., 2016), and it was recently shown that zebrafish lacking ASC are more susceptible to *Salmonella enterica* Typhimurium infection (Tyrkalska et al., 2016). In our case, a live imaging approach allowed us to characterize inflammasome signaling in the skin in vivo. In both fish and mammals, the skin functions as an immune organ that provides a crucial protective barrier (Rakers et al., 2010). Keratinocytes both relay environmental signals to immune cells and execute a response themselves, with their death acting as a potent trigger of skin inflammation (Pasparakis et al., 2014; Peeters et al., 2015). Inflammasome activation in keratinocytes has been implicated in response to several stimuli (Feldmeyer et al., 2007, 2010; Watanabe et al., 2007; Dai et al., 2011; Reinholz et al., 2013; Weinheimer-Haus et al., 2015), and the strong expression of ASC we observed in the skin, as well as other epithelia-like gills and intestines, suggested that the activation of inflammasome is of particular importance in those tissues. Our finding that keratinocytes respond to inflammatory conditions by forming ASC specks and triggering pyroptosis underscores the relevance of inflammasome signaling in epithelia in vivo.

Our work shows that the specific structural mechanisms that lead to ASC assembly into specks are conserved between zebrafish and mammals. First, several different ways of overexpressing ASC in vivo confirmed its high tendency for aggregation, consistent with previous examples showing zebrafish ASC specks in mammalian cells (Masumoto et al., 2003) and in uninfected control zebrafish larvae injected with *asc–GFP* mRNA (Vincent et al., 2016). Second, the abrogation of speck formation when predicted, conserved phosphorylation sites of zebrafish ASC are mutated suggests conservation of JNK and Syk-dependent posttranslational regulatory mechanisms of ASC (Hara et al., 2013; Lin et al., 2015). Last, our CLEM analysis, which constitutes the first structural analysis of in vivo specks, shows their clustered, filamentous nature and confirms the model based on in vitro inflammasome reconstitutions depicting a speck as a three-dimensional, globular ultrastructure composed of multiple, highly intercrossed filaments (Lu et al., 2014).

An important difference between mammalian and zebrafish ASC is the domain that interacts with the effector caspase. In contrast to the mammalian inflammasome, in which Caspase-1 and ASC interact via their CARD domains, zebrafish Caspa, which has an N-terminal PYD instead of a CARD, is recruited to the ASC speck via its PYD domain, in agreement with previous mammalian cell culture experiments (Masumoto et al., 2003). $CARD_A$ in mammals is located on the surface of ASC filaments, enabling the recruitment of Caspase-1. Because CARD domains can themselves assemble into filaments, as in the case of MAVS in RIG-I antiviral signaling (Cai et al., 2016), the ASC filament domain structure could be inverted in zebrafish, allowing the PYD to interact with Caspa. Both amphibians and teleost fish lack the Gasdermin family genes (Tamura et al., 2007). It remains to be investigated whether members of the closely related DFNA5 family, which is present in zebrafish, act as effectors downstream of Caspa in causing pyroptosis.

Our results on the effects of expressing the individual domains of ASC reveal a correlation between the compaction of the ASC speck and the efficiency with which it leads to cell death. Both PYD_A and $CARD_A$ alone have the capacity to aggregate when overexpressed, but neither cluster in a single, compact speck. $CARD_A$ aggregates have no detrimental effect on cells, but overexpression of only PYD_A, whose aggregates are able recruit Caspa, results in cell death. Therefore, in this setup, the association of CARD and PYD, the formation of a compact speck, or the bridging of PYD to other molecules via CARD are all unessential for cell death as such. Instead, the PYD-mediated recruitment of Caspa appears to be sufficient. However, the finding that the rate of aggregation and cell death are significantly reduced indicates that $CARD_A$ is needed for the highly efficient and rapid triggering of pyroptosis. This could be achieved by maximizing speck compaction though filament cross-linking, as shown in cell culture (Dick et al., 2016; Schmidt et al., 2016), which might cause more rapid and efficient nucleation and clustering of Caspa than PYD aggregates achieve, by recruiting additional accessory molecules to the speck that accelerates Caspa activation or through a combination of both mechanisms.

Specks had been shown to remain as stable aggregates in the extracellular space after ASC overexpression in COS-7 cells and in the supernatant of macrophage cell cultures upon exposure to inflammasome-activating stimuli (Balci-Peynircioglu et al., 2008; Baroja-Mazo et al., 2014; Franklin et al., 2014). In the *Tg(HSE:asc-mKate2)* line, ASC specks persist after the death of the cells and appear to remain associated with the pyroptotic cellular debris, which can be readily engulfed by macrophages,

as is the case in culture for in vitro–assembled specks (Franklin et al., 2014) and PITs (Jorgensen et al., 2016). Macrophages in vivo continuously cleared speck-containing cellular debris, and a single macrophage could contain multiple phagosomes with specks. Furthermore, engulfment led to the degradation of the specks within phagosomes. Franklin et al. (2014) reported that macrophages that engulfed in vitro–assembled specks could undergo pyroptosis after the speck was released into the cytosol and nucleated clustering of the phagocytes' soluble ASC (Franklin et al., 2014), an observation which is supported by recent in vivo data (Sagoo et al., 2016). However, we did not find that a macrophage's ability to clear debris in vivo diminished or that the macrophage was affected by the engulfment of a speck in the short term. It is possible that specks enclosed within ruptured membranes are less-efficient triggers of the phagolysosomal damage that releases them into the cytosol or that, in vivo, additional conditions are required to activate that mechanism of signaling spreading, such as extraordinarily high or sustained organismal inflammation levels. This would explain why extracellular specks are detected in the case of chronic, but not acute, inflammation (Franklin et al., 2014).

We noticed that not all specks that formed in the epidermis were removed. Keratinocytes belonging to the outer epidermal layer (EVL), marked by the *krt4* transgene, were extruded from the epithelium toward the outside of the body. Because they are sloughed off and become separate from the living tissue, macrophages are likely unable to reach and remove their cellular debris.

Recently, speck formation within a tissue was visualized by intravital imaging of macrophages derived from retrovirally transduced, ASC–GFP hematopoietic stem cells in bone marrow chimeric mice (Sagoo et al., 2016). A second study generated a transgenic mouse carrying ASC–citrine, which can be expressed in a lineage-specific manner (Tzeng et al., 2016). Although both studies analyze inflammasome activation within living tissue, they rely on the insertion of an additional copy of ASC–FP expressed under viral promoters for protein visualization; thus, expression levels from the transgene are artificial, and cells that endogenously express *asc* will have an increased concentration of the protein. These disadvantages are circumvented by endogenous tagging of *asc*, as in the *Tg(asc:asc-EGFP)* line, in which ASC–GFP is only present in cells in which it is endogenously expressed and at physiologic levels, thus avoiding activation artifacts. We cannot entirely exclude that the GFP itself influences the behavior of the protein, but that would be a caveat affecting all studies using FPs to visualize ASC live. However, because endogenous inflammasome activation in the context of organismal infection has not been studied live, we believe that the *Tg(asc:asc-EGFP)* line will prove a valuable tool to address this question in vivo.

Materials and methods

Zebrafish care, transgenic lines, and genotyping

Zebrafish were cared for as described previously (Westerfield, 2007). The chemical 1-phenyl-2-thiourea (PTU; Sigma-Aldrich) was added to E3 medium at a concentration of 0.2 mM to inhibit pigmentation. The Tupfel long fin (TL) strain was used as the WT. The following transgenic lines were used: *mpeg1:EGFP*^{gl22Tg} (Ellett et al., 2011), *spi1b:GAL4,UAS:TagRFP*^{hdb2Tg} (Sieger et al., 2012), *lyz:DsRed2*^{nz50Tg} (Hall et al., 2007), *β-actin:NLS-tagBFP* (generated in the lab of D. Gilmour by L. Newton, European Molecular Biology Laboratory Heidelberg, Heidelberg, Germany), *mfap4:Tomato-CAAX*^{xt6Tg} (Cronan et al., 2016), *krt4:GFP*^{gz7Tg}, and *krtt1c19e:Tomato*^{fr34Tg} (Fischer et al., 2014). Lines generated in this study are described below. Genomic DNA (gDNA) was extracted from full larvae or adult fin clips with QuickExtract DNA extraction solution (Epicentre); genotyping was performed with Phusion High-Fidelity DNA polymerase (Thermo Fisher Scientific). All animal experiments described in the present study were conducted under the rules of the European Molecular Biology Laboratory (EMBL) and the guidelines of the European Commission (Directive 2010/63/EU).

Acridine orange staining

Acridine orange is a live dye that has previously been used to label dying cells in live zebrafish embryos (Peri and Nüsslein-Volhard, 2008). Larvae were stained by immersion for 45 min in a 1:1,500 dilution of a 10 mg/ml stock (Sigma-Aldrich) prepared in E3, rinsed to remove excess dye, anesthetized, mounted, and imaged directly afterward. Because the dye is light sensitive, larvae were kept in the dark during staining.

Chemical and inflammatory treatments

For Caspase inhibition, the pan-caspase inhibitor Q-VD-OPh hydrate (Sigma-Aldrich) was resuspended in DMSO at a stock concentration of 10 mM. For caspase inhibition, the compound was added directly to the medium at a concentration of 100 µM. For $CuSO_4$ treatment, 3-dpf larvae were treated with for 1 h with copper (II) sulfate (Sigma-Aldrich) at 25 µM. The compound was washed off, and specks were quantified 1 or 3 h after treatment.

Cloning of expression vectors and expression induction

All expression vectors were coinjected with transposase mRNA (100 ng/µl) in embryos at the one-cell stage. For all heat-shock–driven expression, the fusion protein of interest was cloned into a vector backbone containing a bidirectional heat-shock element (HSE) as promoter (Bajoghli et al., 2004), Tol2 sites for transgenesis, and carrying the *cmlc2:tagRFP* as a transgenic marker (Kwan et al., 2007). To induce expression, injected embryos with red "bleeding heart" expression were heat shocked at 39°C in a heating block at any stage between 2.5 dpf and 3.5 dpf. The *Tg(HSE:asc-mKate2)*^{hdb9Tg} line, designated *Tg(HSE:pycard-mKate2)*^{hdb9Tg}, was generated by raising embryos (F0) carrying the heart marker without exposing them to heat shock. The *ubi:LexPR,LexOP:asc-mKate2* vector containing the LexPR/LexOP transactivation system (Emelyanov and Parinov, 2008) was generated via Gateway recombination cloning (Thermo Fisher Scientific) of *ubi*(p5E)/*LexPR,LexOP*(pME)/*asc-mKate2*(p3E). Expression was induced upon addition of 10 µM Mifepristone (RU486; Sigma-Aldrich).

Site-directed mutagenesis

For site-directed mutagenesis of the *HSE:asc-mKate2*, the QuikChange II XL Site-Directed Mutagenesis kit (Agilent Technologies) was used, according to manufacturer's instructions. To make *HSE:asc-mKate2 asc* ATG morpholino-resistant (*HSE:asc*-mKate2*), a total of 6-bp changes were made with two rounds of site-directed mutagenesis; the first introduced the G6A, A9G, and T12A mutations with one complementary primer pair (5′-GCTTGAATTCACCATGGCAGA GTCATTCAAGGAGCAGCTGCAG-3′), and the second introduced the G18A, G21A, and G24A mutations (5′-CTCAAAAGCCTCCTG CAGTTGTTCTTTGAATGACTCTGCCATGGTG-3′). Specific primer pairs were used to mutate each phosphorylation site: T38A (5′-GGAGGCAGGAACCGCGCGTCGCAAAGTCTGCAATCG AAAAGCTG-3′), Y152F (5′-CATCACAAATGAGGATTTCTGTAC CATTCGTAATAAG-3′), T160A (5′-CCATTCGTAATAAGGAGG

CTCCTCAAAAGAAGATG-3′), and T170A (5′-GAGAGAGTTATT AGCAGGCCCAATCACATG-3′).

Single-guide RNA (sgRNA) and mRNA synthesis

To synthesize the templates for sgRNAs targeting *caspa*, the two-oligo PCR method (Shah et al., 2015) was used. For sgRNAs targeting *asc*, sgRNA-containing plasmids were cloned using oligo annealing (Stemmer et al., 2015). All sgRNAs were transcribed using the MEGAshortscript T7 transcription kit (Ambion). To synthesize mRNA, linearized pCS2 + DNA vector containing the gene of interest was used as template and transcribed with the mMessage mMachine SP6 transcription kit (Ambion). RNA from in vitro transcriptions was purified with the RNA Clean and Concentrator-5 (Zymo Research). mRNAs were injected into embryos at the one-cell stage.

RNA extraction, cDNA synthesis, and RT-PCR

Total RNA was extracted from larvae using TriFast (PEQLAB Biotechnologie), according to manufacturer's instructions. To prevent contamination from gDNA, samples were treated with RQ1 RNase-Free DNase (Promega) and were then repurified using TriFast. To generate first-strand cDNA from the total, extracted RNA was generated using the Superscript III Reverse transcription enzyme (Thermo Fisher Scientific). The cDNA obtained was used directly for RT-PCR using Phusion High-Fidelity DNA polymerase (Thermo Fisher Scientific). The following primers were used: *asc* (forward, 5′-AGTAGC AGATGATCTATTGAGG-3′; reverse, 5′-AGAGCATCATACAAGA CTTCTTTCC-3′), *caspa* (forward, 5′-CAGTCAGCGCCCTGAGCT AAACATG-3′; reverse, 5′-TCAACTGAGCTGGATCCTTCGG-3′), and *ef1a* (forward, 5′-CTTCTCAGGCTGACTGTGC-3′; reverse, 5′-CCGCTAGCATTACCCTCC-3′).

Whole-mount, in situ hybridization; plastic embedding; and sectioning

In situ hybridization was performed essentially as described previously (Thisse and Thisse, 2008). Antisense and sense probes for *asc* and *caspa* coding DNA sequence (CDS) were transcribed in vitro from linearized pCS2 + DNA vector containing the entire CDS of each gene with the DIG RNA labeling kit (Roche) and purified with SigmaSpin Post-Reaction Clean-Up columns (Sigma-Aldrich). BM Purple AP substrate (Roche) was used for staining. Whole-mount, in situ samples were sectioned using the Historesin-embedding kit (Leica Biosystems), according to manufacturer's instructions. Sectioning was performed manually using RM2235 manual rotary microtome (Leica Biosystems).

ASC polyclonal antibody production

ASC polyclonal antibody was generated from the full-length, recombinant ASC, purified from a bacterial expression system. Antigen production and antibody purification were performed by the Protein Expression and Purification Core Facility at EMBL. The rabbit immunization procedure and all animal handling were performed by the Polyclonal Antibody Service at the EMBL Laboratory Animal Resources. Antibody specificity was confirmed with preimmunization serum as a negative control and in the immunostaining pattern in *asc* morphant embryos.

Immunostaining

Two variants of immunostainings were used, depending on the tissue of interest. Immunostainings of myeloid cells were performed, as previously described (Varela et al., 2014). To visualize keratinocyte stainings, a less-abrasive protocol, lacking methanol dehydration, proteinase K treatment, and postfixation steps, was used for epidermis preservation. The following primary antibodies were used: antiASC (1:10^3 dilution), antiGFP (1:10^4 dilution; Santa Cruz Biotechnology, Inc.), or antiLamin B2 (1:200 dilution; Thermo Fisher Scientific). Secondary antibodies (Thermo Fisher Scientific) were coupled to Alexa Fluor 488, 568, and 647 (1:500, 1:500, and 1:300 dilutions, respectively).

Protein extraction and Western blotting

To obtain whole-embryo protein lysate, embryos were sonicated in fresh buffer (10 mM Hepes, pH 7.5, 100 mM KCl, 2 mM $MgCl_2$, 0.1 mM $CaCl_2$, 5 mM EGTA, pH 8.0, 1 mM NaF, 1 mM Na_3VO_4, 0.5% Triton X-100, and protease inhibitor cocktail tablets [1 tablet/10 ml; Roche]). Lysate was cleared by centrifugation, and supernatant was collected and stored after addition of 5× SDS sample buffer (10% SDS, 20% glycerol, 0.2 M Tris-HCl, pH 6.8, 0.05% Bromophenol blue, and 10% β-mercaptoethanol added right before use). Prepared protein samples were separated by SDS-PAGE with the Mini-PRO TEAN vertical electrophoresis cell system (Bio-Rad Laboratories), transferred to a polyvinylidene difluoride membrane (Immobilon-P) in a semidry transfer cell (Bio-Rad Laboratories), probed with anti-ASC (1:10^3 or 1:10^4 dilution) or anti-GFP (1:10^4 dilution; Santa Cruz Biotechnology, Inc.), and developed with the corresponding HRP-coupled secondary antibodies (Jackson ImmunoResearch Laboratories, Inc.). Detection was performed using Luminata Crescendo Western HRP substrate (EMD Millipore).

Imaging

For confocal microscopy, larvae were anesthetized with ethyl *m*-aminobenzoate methanesulfonate by adding the compound to the medium at a concentration of 40 µg/ml and mounting it in 1.3% low–melting-point agarose (PEQLAB Biotechnologie). Imaging of immunostainings was performed with a Leica Biosystems SP8 TCS confocal microscope using dry 20×/0.8 or water 40×/1.1 objectives. Live imaging was performed using Zeiss Biosystems LSM 780 confocal microscope at RT. For time-lapse imaging of epidermal and muscle cells, a 40× water objective was used (LD C-Apochromat 40×/1.1 W Corr M27 or C-Apochromat 40×/1.2 W Corr M27; Zeiss Biosystems). Whole larvae were imaged using a 5× (Plan-Apochromat 5×/0.16 M27; Zeiss Biosystems) or 10× (Plan-Apochromat 10×/0.45 M27; Zeiss Biosystems) as tiles and later stitched.

asc knockdown

Design and synthesis of *asc* ATG morpholino (5′-GCTGCTCCTTGA AAGATTCCGCCAT-3′) was performed by Gene Tools, LLC. Stock morpholino was diluted in nuclease-free H_2O to a concentration of 3 mM and stored at RT. For knockdown experiments, morpholino was injected at a concentration of 0.6 mM. Morpholino was validated by immunostaining and, for in vivo experiments, by a loss of fluorescence after injection in homozygous *Tg(asc:asc-EGFP)* embryos.

Generation of the *Tg(asc:asc-EGFP)^{hdb10Tg}* line

For sgRNA design, guide RNAs that targeted the last exon of *asc* (ENS DARG00000040076) were designed using the CRISPR/Cas9 target online predictor CCTop (http://crispr.cos.uni-heidelberg.de; Stemmer et al., 2015). Two suitable hits, guide 1 (5′-ATTCCTGATGGATGA CCTTG-3′) and guide 2 (5′-ATCTTCACTCAGCATCCTCA-3′), were synthesized using the oligo-annealing method into vector DR274. DR274 was a gift from K. Joung (Addgene, Cambridge, MA; plasmid 42250; Hwang et al., 2013). For sgRNA in vivo validation and to test whether sgRNAs guides 1 and 2 targeted the region of interest in vivo, the guides were individually injected with varying concentrations (15–150 ng/µl) together with 1 µl of Cas9 protein (4 mg/ml) complemented with ∼150 mM KCl into fertilized eggs at the one-cell stage of the zebrafish TL strain. Successful knockdown was verified by sequencing of a 1.3-kb PCR product from the targeted region of *asc* (forward,

5′-CCTGTCTGACCATGTGAACATCTA-3′; reverse, 5′-TTAGCA TTTGTCCTTATCGCAAAC-3′). Donor vectors were constructed via Golden GATEway cloning (Kirchmaier et al., 2013). In short, 50 ng of entry vector (EV) plasmids, numbered 1–6, and a vector backbone were digested with 0.5 µl of BsaI (Fast Digest; Thermo Fisher Scientific) and ligated with 0.5 µl of T4 DNA ligase (30 U/µl; Thermo Fisher Scientific) in several rounds in one continuous reaction of 10 cycles, consisting of 30 min at 37°C and 20 min at 16°C, followed by 5 min of 50°C and 5 min of 80°C to inactivate both enzymes. EV1 included a donor plasmid-specific target site for in vivo plasmid linearization (5′-GGC GAGGGCGATGCCACCTACGG-3′; Stemmer et al., 2015), EV3 contained an *EGFP* CDS with a flexilinker for tagging of *asc*, EV4 was empty, and EV6 contained a stop codon. Homology 5′ and 3′ flanks of different lengths (1 kb for 5′ and 1 or 2 kb for 3′) were amplified from zebrafish gDNA and cloned into empty EV2 and EV5. Flanks were amplified and designed according to the specific Cas9 cleavage sites for guides 1 and 2, as previously reported (Hisano et al., 2015), to increase chances of precise integration. All vectors whose cloning is not mentioned were provided by the J. Wittbrodt laboratory (Heidelberg University, Heidelberg, Germany). For homologous recombination, the *asc* sgRNA guides 1 or 2 (120 ng/µl) and a corresponding donor vector (20–50 ng/µl) were injected with a donor-specific sgRNA for donor in vivo plasmid linearization (150 ng/µl) and 1 µl of Cas9 protein (4 mg/ml) in a solution complemented with ∼150 mM KCl. Larvae were screened at 2 dpf for GFP expression. We observed greater successful recombination rates when using *asc* guide 2 and a donor vector with 5′ and 3′ homology flanks of 1 and 2 kb, respectively. However, the number of positive embryos was low and highly variable, ranging from 1 in 40 to 1 in 200 injected embryos. In total, 18 positive F0 larvae were raised into adulthood and screened for positive integration in the germline by outcrossing with WT fish. One founder, whose F1 progeny carried an allele with a correct insertion of *linker-EGFP* cassette at a rate of 30%, was found. Successful integration was confirmed by amplification of the targeted region in the *asc* locus by PCR and sequencing (SF4). Heterozygous *asc-EGFP/+* embryos were raised and incrossed to obtain homozygous *asc-EGFP* embryos. The official designation of the *Tg(asc:asc-EGFP)*^{hdb10Tg} line is *Tg(pycard:pycard-EGFP)*^{hdb10Tg}.

Generation of *caspa* mutant

For sgRNA design, sgRNAs targeting the first exon of the zebrafish gene *caspa* (ENSDARG00000008165) were designed using the tool at http://crispr.mit.edu (Hsu et al., 2013) and were selected, as reported (Shah et al., 2015). To test whether sgRNAs were targeting the region of interest in vivo, sgRNAs were injected in varying concentrations (120–275 ng/µl), together with 1 µl of in-house (Protein Expression and Purification Facility, EMBL, Heidelberg, Germany), synthesized Cas9 protein (4 mg/ml), complemented with ∼150 mM KCl, into fertilized eggs at the one-cell stage of the zebrafish TL strain. Successful knockdown was verified by sequencing an 800-bp PCR product from the targeted region of *caspa* (forward, 5′-TGGGTTAACTAGGCAAGT CAGGG-3′; reverse, 5′-AGGGTGTATCAGGACTTGGGCCC-3′, or reverse 5′-CCACACATGGGAGGTGTGAA-3′). To screen, embryos were injected with the most-efficient sgRNA (5′-GGACGCTTTAAG TAATATTGGGG-3′) and raised to adulthood to obtain the F0. At 6 wk after fertilization, F0 fish were genotyped by fin clipping. F0 fish showing successful targeting were incrossed, and the F1 generation was raised to adulthood. Through genotyping of the F1 adults, two knockout alleles were found: the *caspa*^{K**} (*caspa*^{hdb12}) allele, carrying a 5′-AAATAATAA-3′ insertion at the expected Cas9 cleavage site, resulting in two stop codons, and the *caspa*$^{\Delta 800}$ (*caspa*^{hdb11}), carrying a deletion of ∼800 bp, including most of the first exon and part of the first intron, which resulted in a nonsense mutation. Heterozygous F1 fish carrying both alleles were incrossed to obtain homozygous mutants with either the *caspa*^{K**} or the *caspa*$^{\Delta 800}$ deletion allele.

CLEM

For CLEM analysis, the embryos were high-pressure frozen (HPM010; ABRA Fluid), using 20% dextran or 20% Ficoll as cryoprotectant. The embryos were pierced with a needle in a cryo-microtome chamber (EM FC6; Leica Biosystems) at −160°C to facilitate freeze substitution (Eltsov et al., 2015). Embryos were then freeze-substituted (EM-AFS2; Leica Biosystems) with 0.1% uranyl acetate in acetone at −90°C for 48 h. The temperature was then raised to −45°C at 3.5°C/h, and samples were further incubated for 5 h. After rinsing in acetone, the samples were infiltrated in Lowicryl HM20 resin, and the temperature was raised to −25°C and left to polymerize under UV light for 48 h at −25°C and for further 9 h, the temperature was gradually raised to 20°C (5°C/h). Thick sections (300 nm) were cut from the polymerized resin block and picked up on carbon-coated mesh grids. The imaging of sections by fluorescence microscopy was performed, as previously described (Kukulski et al., 2011; Avinoam et al., 2015) using a widefield fluorescence microscope (Ti-E; Nikon). Images were collected with mCherry-specific settings, as well as transmitted light.

TEM tomography was acquired with a FEI Tecnai F30 electron microscope. Dual-axis tomograms were obtained using SerialEM (Mastronarde, 2005) and reconstructed in eTomo, part of the IMOD software package (Kremer et al., 1996). Correlation between light and electron micrographs was performed with the plugin ec-CLEM (http://icy.bioimageanalysis.org/plugin/ec-CLEM) of the software platform Icy (de Chaumont et al., 2012). Features visible in both the light and electron microscopy images were manually assigned by clicking. The coordinates of pairs in the two imaging modalities were used to calculate a linear transformation, which allowed mapping of the coordinates of the fluorescent spot of interest (red channel) and to overlay it on the electron micrograph. The tomograms were threshold-segmented with the Microscopy Image Browser platform (Belevich et al., 2016), and the resulting model was loaded into the digital space of Amira for visualization (FEI).

Software

The software Geneious (version 6.1.7r; Biomatters Limited) was used for cloning-strategy design, sequencing data analysis, and sequence alignments. The kinase-specific prediction of phosphorylation sites in zebrafish ASC was performed using the online software GPS (version 2.1.1; Xue et al., 2011), using previously described parameters (Hara et al., 2013). The software Prism (version 6.03; GraphPad Software) was used for all statistical analyses and graphs. Raw images were processed using ImageJ/Fiji (National Institutes of Health) and Imaris (version x64 7.6.4; Bitplane, AG).

Online supplemental material

Fig. S1 shows ASC expression pattern during zebrafish early development and generation of *Tg(asc:asc-EGFP)* line. Fig. S2 shows ASC misexpression in vivo, which results in speck formation and leads to keratinocyte cell death. Fig. S3 shows that, in the presence of endogenous ASC, PYD_A, or $CARD_A$, overexpression leads to speck formation. Fig. S4 shows the consequences of Caspa overexpression and generation of a *caspa* mutant. Table S1 shows the results of JNK and Syk kinase-specific phosphorylation site prediction in zebrafish ASC by the online software GPS version 2.1.1. Video 1 shows time-lapse imaging of endogenous speck formation in the *Tg(asc:asc-EGFP)* line. Video 2 shows time-lapse imaging of speck formation induced by transient overexpression of NLR or ASC. Video 3 shows time-lapse imaging of speck formation in full larva and single cells

in the *Tg(HSE:asc-mKate2)* line. Video 4 shows a TEM tomography stack of specks with superposition of manual tracings of individual ASC filaments and their rotation. Video 5 shows time-lapse imaging of induced speck formation in single-muscle cells, EVL keratinocytes, and keratinocytes with plasma membrane labeling. Video 6 shows time-lapse imaging of nuclear speck formation. Video 7 shows time-lapse imaging of macrophages engulfing and digesting specks. Video 8 shows time-lapse imaging of PYD_A or $CARD_A$ transient expression in wild-type and *asc* morphant larvae. Video 9 shows time-lapse imaging of transient expression of ASC in wild-type and *caspa* mutant larvae.

Acknowledgments

We thank B. Bajoghli for helpful discussion and S. Kraus for technical assistance. We are grateful to F. Peri for zebrafish hosting and J.N. Buffoni and C. Henkel for caretaking, to M. Hammerschmidt for sharing the *Tg(krtt1c19e:Tomato)* and *Tg(krt4:GFP)* zebrafish lines, and to D. Gilmour for the *Tg(βactin:NLS-tagBFP)* line generated by L. Newton. We thank the EMBL Protein Expression and Purification Facility as well as the EMBL Animal House for their roles in generating the zebrafish ASC antibody, the EMBL Advanced Light Microscopy Facility (ALMF) for continuous support and Zeiss for support of the AMLF. We are grateful to D. Gilmour, A. Meijer, and F. Peri for comments on this manuscript.

The laboratory of M. Leptin is supported by the European Molecular Biology Organization and the European Molecular Biology Laboratory. P. Kuri was supported by Marie-Curie Initial Training Network FishForPharma FP7-PEOPLE-2011-ITN (grant PITN-GA-2011-289209). N.L. Schieber and Y. Schwab are supported by the European Molecular Biology Laboratory. The laboratory of J. Wittbrodt is supported by Heidelberg University and by the European Union Seventh Framework Programme (ERC advanced grant GA 294354-ManISteC).

The authors declare no competing financial interests.

Author contributions: P. Kuri and M. Leptin designed the study. P. Kuri generated the *Tg(HSE:asc-mKate2)*, *Tg(asc:asc-EGFP)*, and *caspa*$^{-/-}$ lines and performed all experiments, except CLEM, which was performed with N.L. Schieber and Y. Schwab. T. Thumberger and J. Wittbrodt contributed to initial *Tg(asc:asc-EGFP)* design. P. Kuri and M. Leptin interpreted the data and wrote the paper. All authors read and edited the manuscript.

Submitted: 14 March 2017
Revised: 31 May 2017
Accepted: 13 June 2017

References

Angosto, D., and V. Mulero. 2014. The zebrafish as a model to study the inflammasome. *Inflammasome.* 1. http://dx.doi.org/10.2478/infl-2014-0002

Avinoam, O., M. Schorb, C.J. Beese, J.A.G. Briggs, and M. Kaksonen. 2015. Endocytic sites mature by continuous bending and remodeling of the clathrin coat. *Science.* 348:1369–1372. http://dx.doi.org/10.1126/science.aaa9555

Bajoghli, B., N. Aghaallaei, T. Heimbucher, and T. Czerny. 2004. An artificial promoter construct for heat-inducible misexpression during fish embryogenesis. *Dev. Biol.* 271:416–430. http://dx.doi.org/10.1016/j.ydbio.2004.04.006

Balci-Peynircioglu, B., A.L. Waite, P. Schaner, Z.E. Taskiran, N. Richards, D. Orhan, S. Gucer, S. Ozen, D. Gumucio, and E. Yilmaz. 2008. Expression of ASC in renal tissues of familial mediterranean fever patients with amyloidosis: postulating a role for ASC in AA type amyloid deposition. *Exp. Biol. Med. (Maywood).* 233:1324–1333. http://dx.doi.org/10.3181/0803-RM-106

Baroja-Mazo, A., F. Martín-Sánchez, A.I. Gomez, C.M. Martínez, J. Amores-Iniesta, V. Compan, M. Barberà-Cremades, J. Yagüe, E. Ruiz-Ortiz, J. Antón, et al. 2014. The NLRP3 inflammasome is released as a particulate danger signal that amplifies the inflammatory response. *Nat. Immunol.* 15:738–748. http://dx.doi.org/10.1038/ni.2919

Beilharz, M., D. De Nardo's, E. Latz, and B.S. Franklin. 2016. Measuring NLR oligomerization II: Detection of ASC speck formation by confocal microscopy and immunofluorescence. *Methods Mol. Biol.* 1417:145–158. http://dx.doi.org/10.1007/978-1-4939-3566-6_9

Belevich, I., M. Joensuu, D. Kumar, H. Vihinen, and E. Jokitalo. 2016. Microscopy image browser: A platform for segmentation and analysis of multidimensional datasets. *PLoS Biol.* 14:e1002340. http://dx.doi.org/10.1371/journal.pbio.1002340

Broz, P., and V.M. Dixit. 2016. Inflammasomes: Mechanism of assembly, regulation and signalling. *Nat. Rev. Immunol.* 16:407–420. http://dx.doi.org/10.1038/nri.2016.58

Cai, X., J. Chen, H. Xu, S. Liu, Q.-X. Jiang, R. Halfmann, and Z.J. Chen. 2014. Prion-like polymerization underlies signal transduction in antiviral immune defense and inflammasome activation. *Cell.* 156:1207–1222. http://dx.doi.org/10.1016/j.cell.2014.01.063

Cai, X., H. Xu, and Z.J. Chen. 2016. Prion-like polymerization in immunity and inflammation. *Cold Spring Harb. Perspect. Biol.* 9:a023580. http://dx.doi.org/10.1101/cshperspect.a023580

Cheng, J., A.L. Waite, E.R. Tkaczyk, K. Ke, N. Richards, A.J. Hunt, and D.L. Gumucio. 2010. Kinetic properties of ASC protein aggregation in epithelial cells. *J. Cell. Physiol.* 222:738–747.

Cronan, M.R., R.W. Beerman, A.F. Rosenberg, J.W. Saelens, M.G. Johnson, S.H. Oehlers, D.M. Sisk, K.L. Jurcic Smith, N.A. Medvitz, S.E. Miller, et al. 2016. Macrophage epithelial reprogramming underlies mycobacterial granuloma formation and promotes infection. *Immunity.* 45:861–876. http://dx.doi.org/10.1016/j.immuni.2016.09.014

d'Alençon, C.A., O.A. Peña, C. Wittmann, V.E. Gallardo, R.A. Jones, F. Loosli, U. Liebel, C. Grabher, and M.L. Allende. 2010. A high-throughput chemically induced inflammation assay in zebrafish. *BMC Biol.* 8:151. http://dx.doi.org/10.1186/1741-7007-8-151

Dai, X., K. Sayama, M. Tohyama, Y. Shirakata, Y. Hanakawa, S. Tokumaru, L. Yang, S. Hirakawa, and K. Hashimoto. 2011. Mite allergen is a danger signal for the skin via activation of inflammasome in keratinocytes. *J. Allergy Clin. Immunol.* 127:806-14.e1–4. http://dx.doi.org/10.1016/j.jaci.2010.12.006

de Alba, E. 2009. Structure and interdomain dynamics of apoptosis-associated speck-like protein containing a CARD (ASC). *J. Biol. Chem.* 284:32932–32941. http://dx.doi.org/10.1074/jbc.M109.024273

de Chaumont, F., S. Dallongeville, N. Chenouard, N. Hervé, S. Pop, T. Provoost, V. Meas-Yedid, P. Pankajakshan, T. Lecomte, Y. Le Montagner, et al. 2012. Icy: an open bioimage informatics platform for extended reproducible research. *Nat. Methods.* 9:690–696. http://dx.doi.org/10.1038/nmeth.2075

Dick, M.S., L. Sborgi, S. Rühl, S. Hiller, and P. Broz. 2016. ASC filament formation serves as a signal amplification mechanism for inflammasomes. *Nat. Commun.* 7:11929. http://dx.doi.org/10.1038/ncomms11929

Drexler, S.K., L. Bonsignore, M. Masin, A. Tardivel, R. Jackstadt, H. Hermeking, P. Schneider, O. Gross, J. Tschopp, and A.S. Yazdi. 2012. Tissue-specific opposing functions of the inflammasome adaptor ASC in the regulation of epithelial skin carcinogenesis. *Proc. Natl. Acad. Sci. USA.* 109:18384–18389. http://dx.doi.org/10.1073/pnas.1209171109

Ellett, F., L. Pase, J.W. Hayman, A. Andrianopoulos, and G.J. Lieschke. 2011. *mpeg1* promoter transgenes direct macrophage-lineage expression in zebrafish. *Blood.* 117:e49–e56. http://dx.doi.org/10.1182/blood-2010-10-314120

Eltsov, M., N. Dubé, Z. Yu, L. Pasakarnis, U. Haselmann-Weiss, D. Brunner, and A.S. Frangakis. 2015. Quantitative analysis of cytoskeletal reorganization during epithelial tissue sealing by large-volume electron tomography. *Nat. Cell Biol.* 17:605–614. http://dx.doi.org/10.1038/ncb3159

Emelyanov, A., and S. Parinov. 2008. Mifepristone-inducible LexPR system to drive and control gene expression in transgenic zebrafish. *Dev. Biol.* 320:113–121. http://dx.doi.org/10.1016/j.ydbio.2008.04.042

Feldmeyer, L., M. Keller, G. Niklaus, D. Hohl, S. Werner, and H.-D. Beer. 2007. The inflammasome mediates UVB-induced activation and secretion of interleukin-1β by keratinocytes. *Curr. Biol.* 17:1140–1145. http://dx.doi.org/10.1016/j.cub.2007.05.074

Feldmeyer, L., S. Werner, L.E. French, and H.-D. Beer. 2010. Interleukin-1, inflammasomes and the skin. *Eur. J. Cell Biol.* 89:638–644. http://dx.doi.org/10.1016/j.ejcb.2010.04.008

Fernandes-Alnemri, T., J. Wu, J.-W. Yu, P. Datta, B. Miller, W. Jankowski, S. Rosenberg, J. Zhang, and E.S. Alnemri. 2007. The pyroptosome: A supramolecular assembly of ASC dimers mediating inflammatory cell

death via caspase-1 activation. *Cell Death Differ.* 14:1590–1604. http://dx.doi.org/10.1038/sj.cdd.4402194

Fischer, B., M. Metzger, R. Richardson, P. Knyphausen, T. Ramezani, R. Franzen, E. Schmelzer, W. Bloch, T.J. Carney, and M. Hammerschmidt. 2014. p53 and TAp63 promote keratinocyte proliferation and differentiation in breeding tubercles of the zebrafish. *PLoS Genet.* 10:e1004048. http://dx.doi.org/10.1371/journal.pgen.1004048

Franklin, B.S., L. Bossaller, D. De Nardo, J.M. Ratter, A. Stutz, G. Engels, C. Brenker, M. Nordhoff, S.R. Mirandola, A. Al-Amoudi, et al. 2014. The adaptor ASC has extracellular and 'prionoid' activities that propagate inflammation. *Nat. Immunol.* 15:727–737. http://dx.doi.org/10.1038/ni.2913

Hall, C., M.V. Flores, T. Storm, K. Crosier, and P. Crosier. 2007. The zebrafish lysozyme C promoter drives myeloid-specific expression in transgenic fish. *BMC Dev. Biol.* 7:42. http://dx.doi.org/10.1186/1471-213X-7-42

Hansen, J.D., L.N. Vojtech, and K.J. Laing. 2011. Sensing disease and danger: a survey of vertebrate PRRs and their origins. *Dev. Comp. Immunol.* 35:886–897. http://dx.doi.org/10.1016/j.dci.2011.01.008

Hara, H., K. Tsuchiya, I. Kawamura, R. Fang, E. Hernandez-Cuellar, Y. Shen, J. Mizuguchi, E. Schweighoffer, V. Tybulewicz, and M. Mitsuyama. 2013. Phosphorylation of the adaptor ASC acts as a molecular switch that controls the formation of speck-like aggregates and inflammasome activity. *Nat. Immunol.* 14:1247–1255. http://dx.doi.org/10.1038/ni.2749

Hauenstein, A.V., L. Zhang, and H. Wu. 2015. The hierarchical structural architecture of inflammasomes, supramolecular inflammatory machines. *Curr. Opin. Struct. Biol.* 31:75–83. http://dx.doi.org/10.1016/j.sbi.2015.03.014

Hernandez, P.P., C. Undurraga, V.E. Gallardo, N. Mackenzie, M.L. Allende, and A.E. Reyes. 2011. Sublethal concentrations of waterborne copper induce cellular stress and cell death in zebrafish embryos and larvae. *Biol. Res.* 44:7–15. http://dx.doi.org/10.4067/S0716-97602011000100002

Hisano, Y., T. Sakuma, S. Nakade, R. Ohga, S. Ota, H. Okamoto, T. Yamamoto, and A. Kawahara. 2015. Precise in-frame integration of exogenous DNA mediated by CRISPR/Cas9 system in zebrafish. *Sci. Rep.* 5:8841. http://dx.doi.org/10.1038/srep08841

Hoss, F., J.F. Rodriguez-Alcazar, and E. Latz. 2017. Assembly and regulation of ASC specks. *Cell. Mol. Life Sci.* 74:1211–1229. http://dx.doi.org/10.1007/s00018-016-2396-6

Howe, K., P.H. Schiffer, J. Zielinski, T. Wiehe, G.K. Laird, J.C. Marioni, O. Soylemez, F. Kondrashov, and M. Leptin. 2016. Structure and evolutionary history of a large family of NLR proteins in the zebrafish. *Open Biol.* 6:160009. http://dx.doi.org/10.1098/rsob.160009

Hsu, P.D., D.A. Scott, J.A. Weinstein, F.A. Ran, S. Konermann, V. Agarwala, Y. Li, E.J. Fine, X. Wu, O. Shalem, et al. 2013. DNA targeting specificity of RNA-guided Cas9 nucleases. *Nat. Biotechnol.* 31:827–832. http://dx.doi.org/10.1038/nbt.2647

Hwang, W.Y., Y. Fu, D. Reyon, M.L. Maeder, S.Q. Tsai, J.D. Sander, R.T. Peterson, J.-R.J. Yeh, and J.K. Joung. 2013. Efficient genome editing in zebrafish using a CRISPR-Cas system. *Nat. Biotechnol.* 31:227–229. http://dx.doi.org/10.1038/nbt.2501

Jorgensen, I., Y. Zhang, B.A. Krantz, and E.A. Miao. 2016. Pyroptosis triggers pore-induced intracellular traps (PITs) that capture bacteria and lead to their clearance by efferocytosis. *J. Exp. Med.* 213:2113–2128. http://dx.doi.org/10.1084/jem.20151613

Kagan, J.C., V.G. Magupalli, and H. Wu. 2014. SMOCs: Supramolecular organizing centres that control innate immunity. *Nat. Rev. Immunol.* 14:821–826. http://dx.doi.org/10.1038/nri3757

Kirchmaier, S., K. Lust, and J. Wittbrodt. 2013. Golden GATEway cloning—A combinatorial approach to generate fusion and recombination constructs. *PLoS One.* 8:e76117. http://dx.doi.org/10.1371/journal.pone.0076117

Kremer, J.R., D.N. Mastronarde, and J.R. McIntosh. 1996. Computer visualization of three-dimensional image data using IMOD. *J. Struct. Biol.* 116:71–76. http://dx.doi.org/10.1006/jsbi.1996.0013

Kukulski, W., M. Schorb, S. Welsch, A. Picco, M. Kaksonen, and J.A.G. Briggs. 2011. Correlated fluorescence and 3D electron microscopy with high sensitivity and spatial precision. *J. Cell Biol.* 192:111–119. http://dx.doi.org/10.1083/jcb.201009037

Kuri, P., K. Ellwanger, T.A. Kufer, M. Leptin, and B. Bajoghli. 2016. A high-sensitivity, bi-directional reporter to monitor NF-κB activity in cell culture and zebrafish in real-time. *J. Cell Sci.* 130:648–657. http://dx.doi.org/10.1242/jcs.196485

Kwan, K.M., E. Fujimoto, C. Grabher, B.D. Mangum, M.E. Hardy, D.S. Campbell, J.M. Parant, H.J. Yost, J.P. Kanki, and C.-B. Chien. 2007. The Tol2kit: a multisite gateway-based construction kit for Tol2 transposon transgenesis constructs. *Dev. Dyn.* 236:3088–3099. http://dx.doi.org/10.1002/dvdy.21343

Lin, C.-Y., C.-Y. Chiang, and H.-J. Tsai. 2016. Zebrafish and medaka: New model organisms for modern biomedical research. *J. Biomed. Sci.* 23:19. http://dx.doi.org/10.1186/s12929-016-0236-5

Lin, Y.-C., D.-Y. Huang, J.-S. Wang, Y.-L. Lin, S.-L. Hsieh, K.-C. Huang, and W.-W. Lin. 2015. Syk is involved in NLRP3 inflammasome-mediated caspase-1 activation through adaptor ASC phosphorylation and enhanced oligomerization. *J. Leukoc. Biol.* 97:825–835. http://dx.doi.org/10.1189/jlb.3HI0814-371RR

Lu, A., and H. Wu. 2015. Structural mechanisms of inflammasome assembly. *FEBS J.* 282:435–444. http://dx.doi.org/10.1111/febs.13133

Lu, A., V.G. Magupalli, J. Ruan, Q. Yin, M.K. Atianand, M.R. Vos, G.F. Schröder, K.A. Fitzgerald, H. Wu, and E.H. Egelman. 2014. Unified polymerization mechanism for the assembly of ASC-dependent inflammasomes. *Cell.* 156:1193–1206. http://dx.doi.org/10.1016/j.cell.2014.02.008

Man, S.M., and T.-D. Kanneganti. 2016. Converging roles of caspases in inflammasome activation, cell death and innate immunity. *Nat. Rev. Immunol.* 16:7–21. http://dx.doi.org/10.1038/nri.2015.7

Mastronarde, D.N. 2005. Automated electron microscope tomography using robust prediction of specimen movements. *J. Struct. Biol.* 152:36–51. http://dx.doi.org/10.1016/j.jsb.2005.07.007

Masumoto, J., S. Taniguchi, K. Ayukawa, H. Sarvotham, T. Kishino, N. Niikawa, E. Hidaka, T. Katsuyama, T. Higuchi, and J. Sagara. 1999. ASC, a novel 22-kDa protein, aggregates during apoptosis of human promyelocytic leukemia HL-60 cells. *J. Biol. Chem.* 274:33835–33838. http://dx.doi.org/10.1074/jbc.274.48.33835

Masumoto, J., S. Taniguchi, J. Nakayama, M. Shiohara, E. Hidaka, T. Katsuyama, S. Murase, and J. Sagara. 2001. Expression of apoptosis-associated speck-like protein containing a caspase recruitment domain, a pyrin N-terminal homology domain-containing protein, in normal human tissues. *J. Histochem. Cytochem.* 49:1269–1275. http://dx.doi.org/10.1177/002215540104901009

Masumoto, J., W. Zhou, F.F. Chen, F. Su, J.Y. Kuwada, E. Hidaka, T. Katsuyama, J. Sagara, S. Taniguchi, P. Ngo-Hazelett, et al. 2003. Caspy, a zebrafish caspase, activated by ASC oligomerization is required for pharyngeal arch development. *J. Biol. Chem.* 278:4268–4276. http://dx.doi.org/10.1074/jbc.M203944200

Olivari, F.A., P.P. Hernández, and M.L. Allende. 2008. Acute copper exposure induces oxidative stress and cell death in lateral line hair cells of zebrafish larvae. *Brain Res.* 1244:1–12. http://dx.doi.org/10.1016/j.brainres.2008.09.050

Pasparakis, M., I. Haase, and F.O. Nestle. 2014. Mechanisms regulating skin immunity and inflammation. *Nat. Rev. Immunol.* 14:289–301. http://dx.doi.org/10.1038/nri3646

Peeters, P.M., E.F. Wouters, and N.L. Reynaert. 2015. Immune homeostasis in epithelial cells: Evidence and role of inflammasome signaling reviewed. *J. Immunol. Res.* 2015:828264. http://dx.doi.org/10.1155/2015/828264

Peri, F., and C. Nüsslein-Volhard. 2008. Live imaging of neuronal degradation by microglia reveals a role for v0-ATPase a1 in phagosomal fusion in vivo. *Cell.* 133:916–927. http://dx.doi.org/10.1016/j.cell.2008.04.037

Rakers, S., M. Gebert, S. Uppalapati, W. Meyer, P. Maderson, A.F. Sell, C. Kruse, and R. Paus. 2010. 'Fish matters': The relevance of fish skin biology to investigative dermatology. *Exp. Dermatol.* 19:313–324. http://dx.doi.org/10.1111/j.1600-0625.2009.01059.x

Reinholz, M., Y. Kawakami, S. Salzer, A. Kreuter, Y. Dombrowski, S. Koglin, S. Kresse, T. Ruzicka, and J. Schauber. 2013. HPV16 activates the AIM2 inflammasome in keratinocytes. *Arch. Dermatol. Res.* 305:723–732. http://dx.doi.org/10.1007/s00403-013-1375-0

Renshaw, S.A., and N.S. Trede. 2012. A model 450 million years in the making: zebrafish and vertebrate immunity. *Dis. Model. Mech.* 5:38–47. http://dx.doi.org/10.1242/dmm.007138

Sagoo, P., Z. Garcia, B. Breart, F. Lemaître, D. Michonneau, M.L. Albert, Y. Levy, and P. Bousso. 2016. In vivo imaging of inflammasome activation reveals a subcapsular macrophage burst response that mobilizes innate and adaptive immunity. *Nat. Med.* 22:64–71. http://dx.doi.org/10.1038/nm.4016

Santana, P.T., J. Martel, H.C. Lai, J.L. Perfettini, J.M. Kanellopoulos, J.D. Young, R. Coutinho-Silva, and D.M. Ojcius. 2016. Is the inflammasome relevant for epithelial cell function? *Microbes Infect.* 18:93–101. http://dx.doi.org/10.1016/j.micinf.2015.10.007

Sborgi, L., F. Ravotti, V.P. Dandey, M.S. Dick, A. Mazur, S. Reckel, M. Chami, S. Scherer, M. Huber, A. Böckmann, et al. 2015. Structure and assembly of the mouse ASC inflammasome by combined NMR spectroscopy and cryo-electron microscopy. *Proc. Natl. Acad. Sci. USA.* 112:13237–13242. http://dx.doi.org/10.1073/pnas.1507579112

Schmidt, F.I., A. Lu, J.W. Chen, J. Ruan, C. Tang, H. Wu, and H.L. Ploegh. 2016. A single domain antibody fragment that recognizes the adaptor ASC defines the role of ASC domains in inflammasome assembly. *J. Exp. Med.* 213:771–790. http://dx.doi.org/10.1084/jem.20151790

Sester, D.P., S.J. Thygesen, V. Sagulenko, P.R. Vajjhala, J.A. Cridland, N. Vitak, K.W. Chen, G.W. Osborne, K. Schroder, and K.J. Stacey. 2015. A novel flow cytometric method to assess inflammasome formation. *J. Immunol.* 194:455–462. http://dx.doi.org/10.4049/jimmunol.1401110

Shah, A.N., C.F. Davey, A.C. Whitebirch, A.C. Miller, and C.B. Moens. 2015. Rapid reverse genetic screening using CRISPR in zebrafish. *Nat. Methods.* 12:535–540. http://dx.doi.org/10.1038/nmeth.3360

Sharma, D., and T.-D. Kanneganti. 2016. The cell biology of inflammasomes: Mechanisms of inflammasome activation and regulation. *J. Cell Biol.* 213:617–629. http://dx.doi.org/10.1083/jcb.201602089

Sieger, D., C. Moritz, T. Ziegenhals, S. Prykhozhij, and F. Peri. 2012. Long-range Ca^{2+} waves transmit brain-damage signals to microglia. *Dev. Cell.* 22:1138–1148. http://dx.doi.org/10.1016/j.devcel.2012.04.012

Stein, C., M. Caccamo, G. Laird, and M. Leptin. 2007. Conservation and divergence of gene families encoding components of innate immune response systems in zebrafish. *Genome Biol.* 8:R251. http://dx.doi.org/10.1186/gb-2007-8-11-r251

Stemmer, M., T. Thumberger, M. Del Sol Keyer, J. Wittbrodt, and J.L. Mateo. 2015. CCTop: An Intuitive, Flexible and Reliable CRISPR/Cas9 Target Prediction Tool. *PLoS One.* 10:e0124633. http://dx.doi.org/10.1371/journal.pone.0124633

Stutz, A., G.L. Horvath, B.G. Monks, and E. Latz. 2013. ASC speck formation as a readout for inflammasome activation. *Methods Mol. Biol.* 1040:91–101. http://dx.doi.org/10.1007/978-1-62703-523-1_8

Tamura, M., S. Tanaka, T. Fujii, A. Aoki, H. Komiyama, K. Ezawa, K. Sumiyama, T. Sagai, and T. Shiroishi. 2007. Members of a novel gene family, *Gsdm*, are expressed exclusively in the epithelium of the skin and gastrointestinal tract in a highly tissue-specific manner. *Genomics.* 89:618–629. http://dx.doi.org/10.1016/j.ygeno.2007.01.003

Thisse, C., and B. Thisse. 2008. High-resolution in situ hybridization to whole-mount zebrafish embryos. *Nat. Protoc.* 3:59–69. http://dx.doi.org/10.1038/nprot.2007.514

Torraca, V., S. Masud, H.P. Spaink, and A.H. Meijer. 2014. Macrophage-pathogen interactions in infectious diseases: New therapeutic insights from the zebrafish host model. *Dis. Model. Mech.* 7:785–797. http://dx.doi.org/10.1242/dmm.015594

Tyrkalska, S.D., S. Candel, D. Angosto, V. Gómez-Abellán, F. Martín-Sánchez, D. García-Moreno, R. Zapata-Pérez, Á. Sánchez-Ferrer, M.P. Sepulcre, P. Pelegrín, and V. Mulero. 2016. Neutrophils mediate *Salmonella* Typhimurium clearance through the GBP4 inflammasome-dependent production of prostaglandins. *Nat. Commun.* 7:12077. http://dx.doi.org/10.1038/ncomms12077

Tzeng, T.-C., S. Schattgen, B. Monks, D. Wang, A. Cerny, E. Latz, K. Fitzgerald, and D.T. Golenbock. 2016. A fluorescent reporter mouse for inflammasome assembly demonstrates an important role for cell-bound and free ASC specks during in vivo infection. *Cell Reports.* 16:571–582. http://dx.doi.org/10.1016/j.celrep.2016.06.011

Vajjhala, P.R., A. Lu, D.L. Brown, S.W. Pang, V. Sagulenko, D.P. Sester, S.O. Cridland, J.M. Hill, K. Schroder, J.L. Stow, et al. 2015. The inflammasome adaptor ASC induces procaspase-8 death effector domain filaments. *J. Biol. Chem.* 290:29217–29230. http://dx.doi.org/10.1074/jbc.M115.687731

van der Vaart, M., H.P. Spaink, and A.H. Meijer. 2012. Pathogen recognition and activation of the innate immune response in zebrafish. *Adv. Hematol.* 2012:159807. http://dx.doi.org/10.1155/2012/159807

Vande Walle, L., and M. Lamkanfi. 2016. Pyroptosis. *Curr. Biol.* 26:R568–R572. http://dx.doi.org/10.1016/j.cub.2016.02.019

Varela, M., A. Romero, S. Dios, M. van der Vaart, A. Figueras, A.H. Meijer, and B. Novoa. 2014. Cellular visualization of macrophage pyroptosis and interleukin-1β release in a viral hemorrhagic infection in zebrafish larvae. *J. Virol.* 88:12026–12040. http://dx.doi.org/10.1128/JVI.02056-14

Vince, J.E., and J. Silke. 2016. The intersection of cell death and inflammasome activation. *Cell. Mol. Life Sci.* 73:2349–2367. http://dx.doi.org/10.1007/s00018-016-2205-2

Vincent, W.J.B., C.M. Freisinger, P.-Y. Lam, A. Huttenlocher, and J.-D. Sauer. 2016. Macrophages mediate flagellin induced inflammasome activation and host defense in zebrafish. *Cell. Microbiol.* 18:591–604. http://dx.doi.org/10.1111/cmi.12536

Vojtech, L.N., N. Scharping, J.C. Woodson, and J.D. Hansen. 2012. Roles of inflammatory caspases during processing of zebrafish interleukin-1β in Francisella noatunensis infection. *Infect. Immun.* 80:2878–2885. http://dx.doi.org/10.1128/IAI.00543-12

Watanabe, H., O. Gaide, V. Pétrilli, F. Martinon, E. Contassot, S. Roques, J.A. Kummer, J. Tschopp, and L.E. French. 2007. Activation of the IL-1β-processing inflammasome is involved in contact hypersensitivity. *J. Invest. Dermatol.* 127:1956–1963. http://dx.doi.org/10.1038/sj.jid.5700819

Weinheimer-Haus, E.M., R.E. Mirza, and T.J. Koh. 2015. Nod-like receptor protein-3 inflammasome plays an important role during early stages of wound healing. *PLoS One.* 10:e0119106. http://dx.doi.org/10.1371/journal.pone.0119106

Westerfield, M. 2007. The Zebrafish Book. University of Oregon Press, Eugene, OR. 396 pp.

Xue, Y., Z. Liu, J. Cao, Q. Ma, X. Gao, Q. Wang, C. Jin, Y. Zhou, L. Wen, and J. Ren. 2011. GPS 2.1: Enhanced prediction of kinase-specific phosphorylation sites with an algorithm of motif length selection. *Protein Eng. Des. Sel.* 24:255–260. http://dx.doi.org/10.1093/protein/gzq094

Yazdi, A.S., S.K. Drexler, and J. Tschopp. 2010. The role of the inflammasome in nonmyeloid cells. *J. Clin. Immunol.* 30:623–627. http://dx.doi.org/10.1007/s10875-010-9437-y